STRUCTURAL CHEMISTRY

ISSN: 2053-2296
journals.iucr.org/c

Recent advances in isopolyoxotungstates and their derivatives

Ya-Jie Liu, Meng-Tian Jin, Li-Juan Chen and Jun-Wei Zhao

Acta Cryst. (2018). C**74**, 1202–1221

Acta Cryst C STRUCTURAL CHEMISTRY

ISSN 2053-2296

Recent advances in isopolyoxotungstates and their derivatives

Ya-Jie Liu, Meng-Tian Jin, Li-Juan Chen* and Jun-Wei Zhao*

Henan Key Laboratory of Polyoxometalate Chemistry, College of Chemistry and Chemical Engineering, Henan University, Kaifeng 475004, Henan Province, People's Republic of China. *Correspondence e-mail: ljchen@henu.edu.cn, zhaojunwei@henu.edu.cn

Received 28 April 2018
Accepted 4 September 2018

Edited by J. R. Galán-Mascarós, Institute of Chemical Research of Catalonia (ICIQ), Spain

Keywords: polyoxometalate; isopolyoxotungstate; synthesis; structure; crystal structure.

Supporting information: this article has supporting information at journals.iucr.org/c

During the past decade, isopolyoxotungstates (iso-POTs) and their derivatives have been greatly developed due to their unique structures and potential applications in luminescence, magnetism, catalysis *etc.* This brief review is principally focused on the main research progress on iso-POTs, iso-POT-based transition-metal derivatives, iso-POT-based rare-earth derivatives, iso-POT-based organometallic derivatives and iso-POT-based heterometallic derivatives, and gives a summary of some representative examples of their syntheses, structures and related properties. In addition, an outlook on the future of this area is presented in the final section. We believe that this systematic commentary on iso-POTs and their derivatives will not only disclose a rich set of iso-POT structures, but also reveal a more promising direction for the further functionalization of iso-POTs.

1. Introduction

Polyoxometalates (POMs), as a unique and important class of discrete anionic oxide clusters, are formed by oxo-bridging early transition-metal atoms in their d^0 or d^1 electronic configurations (usually $Mo^{VI/V}$, $W^{VI/V}$, V^V, Nb^V or Ta^V) (Long *et al.*, 2010; Mitchell *et al.*, 2011; Zhang *et al.*, 2016; Zhao, Li, Ma *et al.*, 2016). These high-oxidation metal atoms are coordinated by oxygen ligands, giving rise to $\{MO_x\}$ (x = 4–7) geometries and the resulting $\{MO_x\}$ units are further joined together by corner-, edge- or face-sharing O atoms (formally O^{2-} or occasionally HO^- ions) (Ma *et al.*, 2015, 2018; Reinoso *et al.*, 2010). The studies on POM chemistry date back to the discovery of the first POM cluster (the ammonium salt of $PMo_{12}O_{40}^{3-}$) in 1826 by Berzelius (Zhao, Li, Chen *et al.*, 2016). Then, with the development of the X-ray diffraction technique, accurate structural information on crystalline POM-based materials could be obtained, which not only provided accurate structural data for mechanism explanation and theoretical calculation, but also afforded the necessary guidance for the bottom-up assembly of a variety of novel functional POM-based materials (Coppens *et al.*, 2014; Rozes & Sanchez, 2011).

As one classical and representative member of the POM family, systematic studies on polyoxotungstates (POTs) have established standards for the bottom-up assembly of cluster-based crystalline materials which exhibit excellent performance in a wide range of applications because of their appealing electronic and molecular properties, such as magnetism, catalysis, medicine or materials science (Chen, Yan *et al.*, 2014; Gao *et al.*, 2012; Kortz *et al.*, 2009; Xin & Pope, 1996; Zhang *et al.*, 2016). Currently, the development of new POT structures has thus far mostly involved the integration of

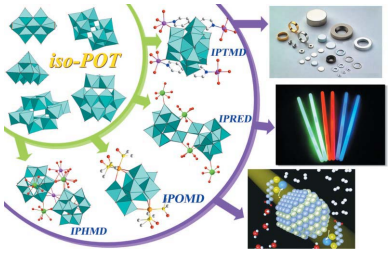

heteroatoms into tungstate-based frameworks, namely, heteropolyoxotungstates (hetero-POTs) with the general formula $[X_pW_qO_y]^{n-}$, in which *X* represents the heteroatoms (*e.g.* P^V, Si^{IV}, Ge^{IV}, As^V *etc.*) (Miras *et al.*, 2008). The vast growth in the number of hetero-POTs with an unmatched range of physical and chemical properties may be rooted in the following reasons: (i) hetero-POTs could be obtained easily by simple acidification in one- or two-step processes in high yield due to the template-inducing effect of heteroatoms (*e.g.* PO_4^{3-}, AsO_4^{3-}, SiO_4^{3-}, GeO_4^{4-}, AsO_3^{3-}, SbO_3^{3-}, IO_6^{5-} *etc.*) (Cameron *et al.*, 2014; Chen *et al.*, 2013); (ii) they can exist over a wide pH range, which is suitable for the existence of transition metal (TM) cations, rare earth (RE) cations or other clusters (Wu *et al.*, 2015); (iii) the stereochemical effect of the lone electron pairs orientated on trigonal pyramidal XO_3 groups (*X* = As^{III}, Sb^{III}, Bi^{III}, Se^{IV} and Te^{IV}) encapsulated at the centres of POMs can to some degree hinder the closure of cage-like POM intermediates forming lacunary hetero-POT building blocks, which favours the self-assembly of large poly(hetero-POT)s (Zhao, Li, Ma *et al.*, 2016); (iv) these lacunary hetero-POT precursors can usually work as excellent multidentate inorganic ligands to coordinate with TM/RE electrophiles generating TM-substituted hetero-POTs, RE-substituted hetero-POTs or even TM–RE heterometal-substituted hetero-POTs (Du *et al.*, 2013; Rodriguez-Albelo *et al.*, 2009). Up to now, abundant functional hetero-POTs were isolated by introduction of TM or RE centres into the defect sites, which almost complete its full coverage of POM chemistry, from purely synthetic strategies aimed at explaining the mechanism of the assembly processes, to the practical research fields that attempt to expand the scope of applications of POMs (Liu *et al.*, 2016). Several important reviews on this area have already been published (Ma *et al.*, 2015, 2016; Oms *et al.*, 2012; Zheng & Yang, 2012). However, isopolyoxotungstates (iso-POTs) composed of a metal oxide framework without internal heteroatoms (Long *et al.*, 2007) are particularly rare and only a handful of examples are known, which may be related to the lack of central heteroatoms in iso-POTs that can be conducive to stabilizing POM structures. Compared with hetero-POTs, the lack of central heteroatoms in iso-POTs can endow a more labile nature on iso-POT building blocks (Li *et al.*, 2016; Long *et al.*, 2010).

Nonetheless, iso-POTs, representing a growing subset of POMs, also have interesting physical properties, such as high charges and strongly basic oxygen surfaces (Long *et al.*, 2007, 2010), which indicates that they are still attractive units for the bottom-up assembly of novel functional POM-based materials. Hitherto, synthetic approaches for the preparation of iso-POTs have been largely developed from traditional aqueous solution synthesis to hydro(solvo)thermal reactions, and even networked reactor systems. There is no doubt that these diverse synthetic methods expand the horizons for the preparation of novel iso-POT crystalline materials and also extend their properties. Up to now, several iso-POTs have been obtained as a result of the unremitting efforts of synthetic chemists, although the ingenious design and synth-

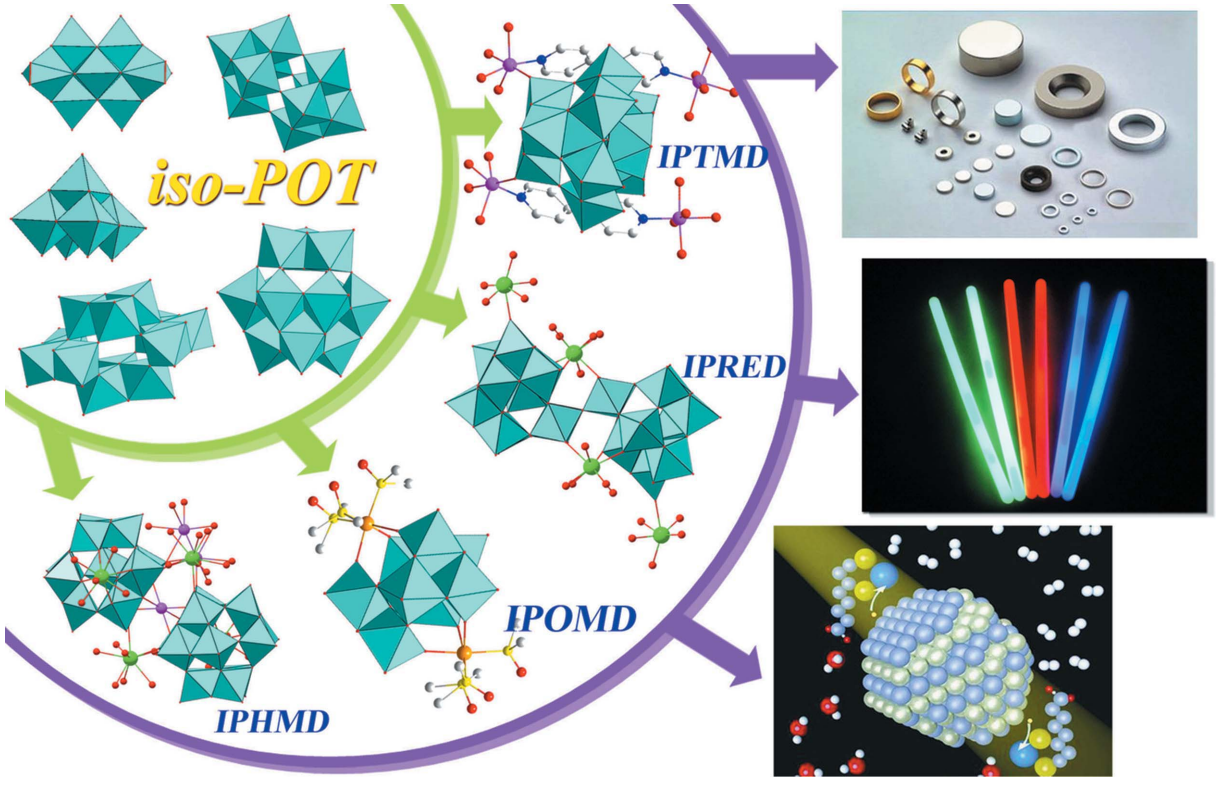

Figure 1
Representative findings of iso-POTs and their derivatives and their potential applications in magnetism, fluorescence and catalysis. Colour key: WO_6 blue, O red, TM (transition metal) pink, RE (rare earth) green, OM (organometallic) orange, S yellow, C grey and N dark blue.

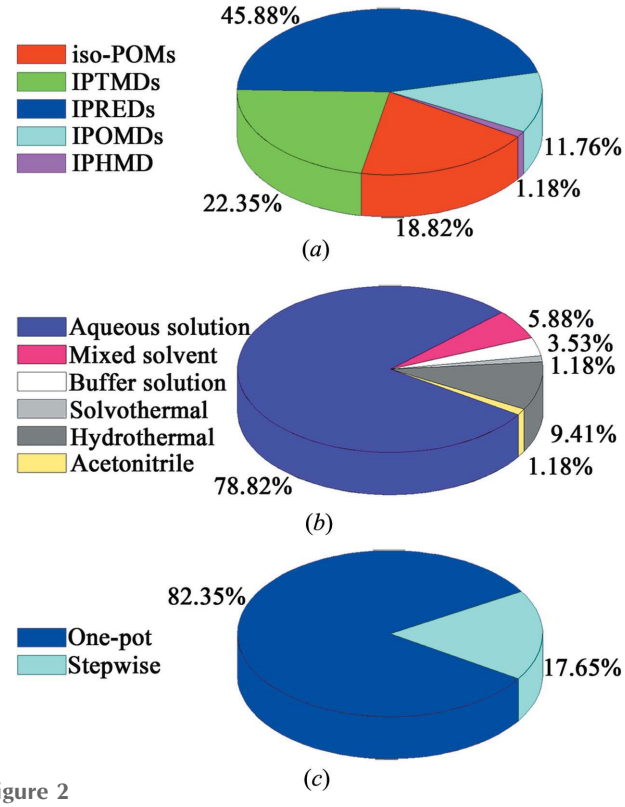

Figure 2
(*a*) Pie chart of the percentage of reported iso-POTs and their derivatives based on their structural types. (*b*) Pie chart of the percentage of reported iso-POTs and their derivatives based on their preparation methods. (*c*) Pie chart of the percentage of reported iso-POTs and their derivatives based on the one-step synthetic strategy and the stepwise synthetic strategy.

esis of novel iso-POTs are still considerably challenging issues, such as the peroxo-containing $[W_4O_8(O_2)_6(CO_3)]^{6-}$ (Stomberg, 1985), Lindqvist-type $[W_6O_{19}]^{2-}$ (Fuchs *et al.*, 1978), S-shaped $[H_2W_{22}O_{74}]^{14-}$ (Ismail, Bassil *et al.*, 2009; Ismail, Dickman & Kortz, 2009), the §-like $[H_{10}W_{34}O_{116}]^{18-}$ clusters (Miras *et al.*, 2008), the triangular $[H_{12}W_{36}O_{120}]^{12-}$ (Long *et al.*, 2004), the Well-Dawson-like $[H_4W_{18}O_{56}(WO_6)]^{6-}$ (Long, Kögerler *et al.*, 2006) and the gigantic $[H_{12}W_{92}O_{311}]^{58-}$ cluster (Zhan *et al.*, 2015). The successful syntheses of these iso-POMs provide the useful building blocks or precursors for constructing novel and huge tungsten–oxo clusters. In addition, with the comprehensive research drive in POM chemistry, the exploration and assembly of multifunctional iso-POT-based derivatives, such as iso-POT-based TM derivatives (IPTMDs), iso-POT-based RE derivatives (IPREDs), iso-POT-based organometallic (OM) derivatives (IPOMDs), as well as iso-POT-based heterometallic (HM) derivatives (IPHMDs), have become a crucial research topic. And the current goal is to develop sophisticated designer molecule-based materials and explore their potential applications in magnetism, catalysis, medicine and photophysics (Figs. 1 and 2*a*). However, since an earlier special issue on POMs published in *Chemical Reviews* by Hill *et al.* in 1998 (Hill, 1998), no critical and comprehensive review of iso-POTs and their derivatives has been reported. We believe that a systematic review of iso-POTs and their derivatives would further benefit the development of this field because the continuous breakthroughs have not ceased in the preparations, modifications and applications of iso-POTs, especially in the last few years.

In this review, we aim to put together the global research efforts and motivate innovative ideas for promoting this area to synthesize gigantic iso-POT-based architectures. Beginning with an introduction describing the latest synthetic approaches, we provide an overview of the development of diverse iso-POT structures and their derivatives modified by various metal ions. Moreover, their tunable properties and growing applications are also reviewed.

2. Synthetic strategies

The absence of direct geometrical control from central heteroatoms and the more labile nature of iso-POT building blocks have hampered the development of iso-POTs in the past several decades. On account of worldwide research efforts, diverse synthetic methods have been developed to accelerate the acquisition of intriguing crystalline iso-POT-based materials (Fig. 2). Hitherto, two main preparation methods were applied to the preparation of iso-POTs and their derivatives, namely, the conventional aqueous solution method and the hydro(solvo)thermal technique. Among them, the conventional aqueous solution method has been extensively used, which can be attributable to the following reasons: (i) mild reaction conditions (T < 373 K, ambient pressure), relatively easy operation, and simple equipment requirements; (ii) the whole reaction process is controllable and observable; (iii) the homogeneous system is conducive to the mutual diffusion of different chemical components and further increases the collision probability between atoms or molecules; (iv) high-quality crystals can be obtained by the slow evaporation process; (v) the products are usually pure and may dissolve in water or common organic solvents, which thus can be conveniently characterized. Meanwhile, the hydro(solvo)thermal technique has also been proved to be a serviceable method in making iso-POT-based crystalline materials, especially for IPTMDs. In comparison to the conventional aqueous solution method, the higher pressure and temperature under hydro(solvo)thermal conditions can enhance the solubility of the starting materials. Therefore, more components can be introduced to the reaction system, which can further enrich the structural diversity and extend functional applications. What is more, the reaction parameters can be easily controlled by setting the oven at different temperatures at required times, and even by changing the warming up and cooling down rate (Fang *et al.*, 2017). In addition, the metastable phases can be easily caught by the hydrothermal method, which are often difficult or impossible to make by other synthetic methods. Hitherto, more than 40 articles on iso-POTs and their derivatives have been published From Fig. 2(*b*), we can see that the conventional aqueous solution synthesis route has been proven to be a more powerful and efficient method for synthesizing iso-POT-based crystalline materials, which may be due to the higher level of

Table 1
A summary of iso-POTs and their derivatives.

Formula	Space group	Preparation method	Synthetic strategy	CCDC/CSD number
Iso-POTs				
$[W_4O_{16}]^{8-}$	$P\bar{1}$	Aqueous solution	One-pot	408189
$[W_4O_8(O_2)_6(CO_3)]^{6-}$	$P2_1/n$	Aqueous solution	One-pot	
$[HW_5O_{19}]^{7-}$	$P\bar{1}$	Aqueous solution	One-pot	405326
$[W_6O_{19}]^{2-}$	$P2_1/c$	Aqueous solution	One-pot	
$[H_3W_6O_{22}]^{5-}$	$P\bar{1}$	Aqueous solution	One-pot	57292
$[\{H(SO_4)W_3O_7(O_2)_2\}_2O]^{4-}$	$C2/c$	Aqueous solution	One-pot	
$[W_7O_{22}(O_2)_2]^{6-}$	$P2_1/c$	Aqueous solution	One-pot	227357
$[W_{10}O_{32}]^{4-}$	$P2_1/n$	Aqueous solution	One-pot	228719
$[H_2W_{12}O_{42}]^{10-}$	$P2_1/n$	Aqueous solution	One-pot	76344
$[H_4W_{19}O_{62}]^{6-}$	$P\bar{1}$	Aqueous solution	One-pot	292393
$[H_4W_{22}O_{74}]^{12-}$	$P\bar{1}$	Aqueous solution	One-pot	425076
$[W_{24}O_{84}]^{24-}$	$P2_1/n$	Aqueous solution	One-pot	408188
$[H_{10}W_{34}O_{116}]^{18-}$	$P\bar{1}$	Aqueous solution	One-pot	419466
$[H_{12}W_{36}O_{120}]^{12-}$	$Pnma$	Aqueous solution	One-pot	289116
$[H_{12}W_{48}O_{164}]^{28-}$	$P2_1/c$	Aqueous solution	One-pot	1036064
$[H_{20}W_{56}O_{190}]^{24-}$	$P\bar{1}$	Aqueous solution	One-pot	1036062
IPTMDs				
$[(CuL)_2(WO_4)_2\{CuL(H_2O)\}_2][W_{10}O_{32}]\cdot 8H_2O$ (L = 4′-(pyridin-2-yl)-2,2′:6′,2″-terpyridine)	$P\bar{1}$	Aqueous solution	Stepwise	892255
$[\{CuL_2\}_2W_{10}O_{32}]\cdot 2H_2O$ (L = 2,2′-bipyridine)	$P\bar{1}$	Aqueous solution	One-pot	194410
$[Cu_2L_2Cl_2]_2[W_{10}O_{32}]$ (L = terpyridine)	$P\bar{1}$	Aqueous solution	Stepwise	
$\{[Cu_2(bpy)(H_2O)_{5.5}]_2[H_2W_{11}O_{38}]\cdot 3H_2O\cdot 0.5CH_3CN\}$ (bpy = 4,4′-bipyridine)	$P2_1/m$	Solvothermal	Stepwise	
$[(Co(H_2O)_4)_2(H_2W_{12}O_{42})]_n^{6n-}$	$P2_1/n$	Aqueous solution	One-pot	
$[Cu(H_2O)_2(H_2W_{12}O_{42})]^{8-}$	$P\bar{1}$	Aqueous solution	One-pot	419058
$[Cd(H_2O)_2(H_2W_{12}O_{42})]^{8-}$	$P\bar{1}$	Aqueous solution	One-pot	419057
$[Cd_{1.3}(H_2O)_2(H_2W_{12}O_{42})]^{7.4-}$	$P\bar{1}$	Buffer solution	One-pot	419056
$[Cu(en)_2]_3[\{Cu(en)_2\}_2(H_2W_{12}O_{42})]\cdot 12H_2O$	$P\bar{1}$	Hydrothermal	One-pot	185816
$[Ni(bpy)_3]_{1.5}[Ni(bpy)_2(H_2O)\{H_3W_{12}O_{40}\}]\cdot 0.5H_2O$ (bpy = 2,2′-bipyridine)	$C2/c$	Hydrothermal	One-pot	194408
$[\{Ni(phen)_2(H_2O)\}_2\{H_4W_{12}O_{40}\}]\cdot 4H_2O$ (phen = *o*-phenanthroline)	$P\bar{1}$	Hydrothermal	One-pot	194409
$[\{Cu(phen)_2\}_4\{H_2W_{12}O_{40}\}][\{Cu(phen)_2\}_2\{H_2W_{12}O_{40}\}]\cdot 3H_2O$ (phen = *o*-phenanthroline)	$P\bar{1}$	Hydrothermal	One-pot	194411
$[Cu_3L_3(H_2O)_2(H_2W_{12}O_{40})]\cdot 4H_2O$ {L = 2-[4,6-bis(pyridin-2-yl)pyridin-2-yl]pyridine}	$P2_12_12_1$	Hydrothermal	Stepwise	
$(CuL)_2[H_4W_{12}O_{40}]\cdot 5H_2O$ {L = 2-[4,6-bis(pyridin-2-yl)pyridin-2-yl]pyridine}	$C2/c$	Hydrothermal	Stepwise	
$[Cu_3L_3(H_2O)(H_2W_{12}O_{40})]_2\cdot 4H_2O$ (L = terpyridine)	$P2_1/c$	Hydrothermal	Stepwise	
$[enH_2]_2[Cu(en)_2]_3[H_2W_{12}O_{42}]\cdot 6H_2O$	$C2/c$	Hydrothermal	One-pot	884009
$[Mn_{14}W_{48}O_{192}H_{20}]^{26-}$	$P\bar{1}$	Aqueous solution	Stepwise	781988
$[(C_2H_8N_2)_4Cu_{16}(H_{12}W_{92}O_{311})]^{26-}$	$C2/c$	Aqueous solution	One-pot	1036063
$[H_{16}Co_8W_{200}O_{660}(H_2O)_{40}]^{88-}$	$P4_2/nmc$	Aqueous solution	One-pot	895471
IPREDs				
$[RE_2(C_2O_4)(H_2O)_4(OH)W_4O_{16}]_2^{10-}$ (RE = Eu^{III}, Ho^{III}, Er^{III} and Tb^{III})	$C2/m$	Aqueous solution	One-pot	995656–995661
$[La(W_5O_{18})_2]^{9-}$	$C2/c$	Aqueous solution	One-pot	
$[Ce(H_2O)(DMF)_6(W_{10}O_{32})]\cdot DMF\cdot CH_3CH_2OH$	$P2_1/n$	Mixed solvent	Stepwise	609253
$[H_6Ce_2(H_2O)Cl(W_5O_{18})_3]^{7-}$	$P2_1/c$	Aqueous solution	One-pot	416677
$[RE(C_2O_4)W_5O_{18})]_4^{20-}$ (RE = Eu^{III}, Ho^{III}, Er^{III} and Tb^{III})	$P\bar{1}$	Aqueous solution	One-pot	1007747–1007748
$[Ce_2(H_2O)_6W_{22}O_{72}(OH)_4]^{10-}$	$C2/c$	Aqueous solution	One-pot	975840
$[RE_2(H_2O)_{10}W_{22}O_{71}(OH)_2]^{8-}$ (RE = La^{III}, Ce^{III}, Tb^{III}, Dy^{III}, Ho^{III}, Er^{III}, Tm^{III}, Yb^{III}, Lu^{III} and Y^{III})	$P\bar{1}$	Aqueous solution	One-pot	
$\{[RE(H_2O)_4][RE(H_2O)_5]_2[W_{22}O_{74}H_2]\}^{5-}$ (RE = Gd^{III}, Tb^{III}, Er^{III}, Tm^{III}, Yb^{III} and Lu^{III})	$P\bar{1}$	Aqueous solution	One-pot	1437597–1437602,
$\{[Eu(H_2O)_7]_2[Eu(H_2O)_5]_2[W_{22}O_{74}H_2]\}^{2-}$	$P\bar{1}$	Aqueous solution	One-pot	1437596
$[RE_2(H_2O)_{10}W_{28}O_{93}(OH)_2]^{14-}$ (RE = Sm^{III} and Eu^{III})	$P\bar{1}$, $P2_1/n$	Aqueous solution	One-pot	
$[Ce_2(H_2O)_{10}W_{28}O_{92}(OH)_2]^{12-}$	$P\bar{1}$	Aqueous solution	One-pot	975842
$[RE_4(WO_4)(H_2O)_{16}\{W_7O_{22}(O_2)_2\}_4]^{14-}$ (RE = La^{III} and Pr^{III})	$I\bar{4}3d$	Aqueous solution	One-pot	425725, 425726
$[Ce_4(H_2O)_{12}W_{44}O_{144}(OH)_{12}]^{24-}$	$I4_1/a$	Aqueous solution	One-pot	975841
$\{[RE_4(H_2O)_{22}W_{28}O_{94}H_2]_2\}^{12-}$ (RE = Pr^{III}, Nd^{III} and Sm^{III})	$P\bar{1}$	Aqueous solution	One-pot	1430481, 1411408, 1411409
$[Ce_2(H_2O)_9W_{36}O_{110}(OH)_{12}]_2^{20-}$	$P\bar{1}$	Aqueous solution	One-pot	975844
IPOMDs				
$[\{Ru(\eta^6\text{-}C_6Me_6)\}_4W_4O_{16}]$	$C2/c$	Acetonitrile solution	Stepwise	160122
$[\{Ru(\eta^6\text{-}C_6Me_6)\}_2W_5O_{18}\{Ru(\eta^6\text{-}C_6Me_6)(H_2O)\}]$	$Pmcn$	Aqueous solution	Stepwise	160124
$[\{(CH_3)_2Sn\}_2(W_6O_{22})]^{4-}$	$C2/c$	Aqueous solution	One-pot	
$\{[H_2W_8O_{30}][M(CO)_3]_2\}^{8-}$ (M = Mn^{I} and Re^{I})	$P\bar{1}$	Mixed solvent	One-pot	809237, 809239

Table 1 (continued)

Formula	Space group	Preparation method	Synthetic strategy	CCDC/CSD number
$[Mn(H_2O)_2\{[H_2W_8O_{30}][M(CO)_3]_2\}]^{6-}$	$P\overline{1}$	Mixed solvent	One-pot	809238
$[\{Ru(C_6H_6)\}_2W_8O_{28}(OH)_2]^{6-}$	$P2_1/n$	Buffer solution	Stepwise	900793
$[\{Ru(\eta^6\text{-}p\text{-}MeC_6H_4{}^iPr)\}_2(\mu\text{-}OH)_3]_2[\{Ru(\eta^6\text{-}p\text{-}MeC_6H_4{}^iPr)\}_2W_8O_{28}(OH)_2\{Ru(\eta^6\text{-}p\text{-}MeC_6H_4{}^iPr)(H_2O)\}_2]$	$P2_1/n$	Aqueous solution	Stepwise	160123
$[HW_9O_{33}Ru^{II}{}_2(dmso)_6]^{7-}$	R_3	Buffer solution	Stepwise	234284
$[Ru(2,2'\text{-bipyridine})_3]_2[W_{10}O_{32}]\cdot 3DMSO$	$P2_1/c$	Mixed solvent	Stepwise	
IPHMDs				
$[\{Ag_3(H_2O)_2\}\{Ce(H_2O)_{12}\}\subset\{H_2W_{11}Ce(H_2O)_4O_{39}\}_2]^{5-}$	$P\overline{1}$	Aqueous solution	Stepwise	

structural and coordinative flexibility when compared to the hydrothermal method.

As for the synthetic strategies, the one-pot self-assembly synthesis of simple WO_4^{2-} and other components is still an important synthetic strategy for the construction of large iso-POTs and their derivatives, although its synthetic mechanism is not well known up to now. Typically, one of the synthetic methods of iso-POT materials is the one-pot reaction strategy, in which some reaction parameters, such as pH, crystal growth time, ionic strength of the solvent and temperature, dramatically affect the final products. Hence, the control of a single reaction parameter can represent a facile and flexible route for the acquisition of novel iso-POT architectures. Under the guidance of such an idea, more and more attention has been paid to the design and synthesis of iso-POT-based crystalline materials *via* one-pot reactions. For example, Cronin and co-workers isolated and crystallized an S-shaped $[H_4W_{22}O_{74}]^{12-}$ cluster at pH 3.4 and a related §-shaped $[H_{10}W_{34}O_{116}]^{18-}$ cluster at pH 2.4 using a combination of pH and anion control (Miras *et al.*, 2008); our group reported two types of oxalate-connected RE-substituted iso-POTs utilizing different alkaline cations. When only Na^+ ions are present in the system, a class of double-oxalate-bridged Lindqvist dimeric RE-substituted iso-POTs, *i.e.* $[RE_2(C_2O_4)(H_2O)_4(OH)W_4O_{16}]_2^{10-}$ (RE = Eu^{III}, Ho^{III}, Er^{III} and Tb^{III}), were found, while when Na^+ and K^+ ions are simultaneously introduced to the system under the same conditions, another class of single-oxalate-connected Lindqvist tetrameric RE-substituted iso-POTs, *i.e.* $[RE(C_2O_4)W_5O_{18}]_4^{20-}$ (RE = Eu^{III}, Ho^{III}, Er^{III} and Tb^{III}), were observed (Zhao *et al.*, 2014). What is more, combining the solution synthesis with the networked reactor system, Cronin's group also proposed a networked one-pot reaction array and

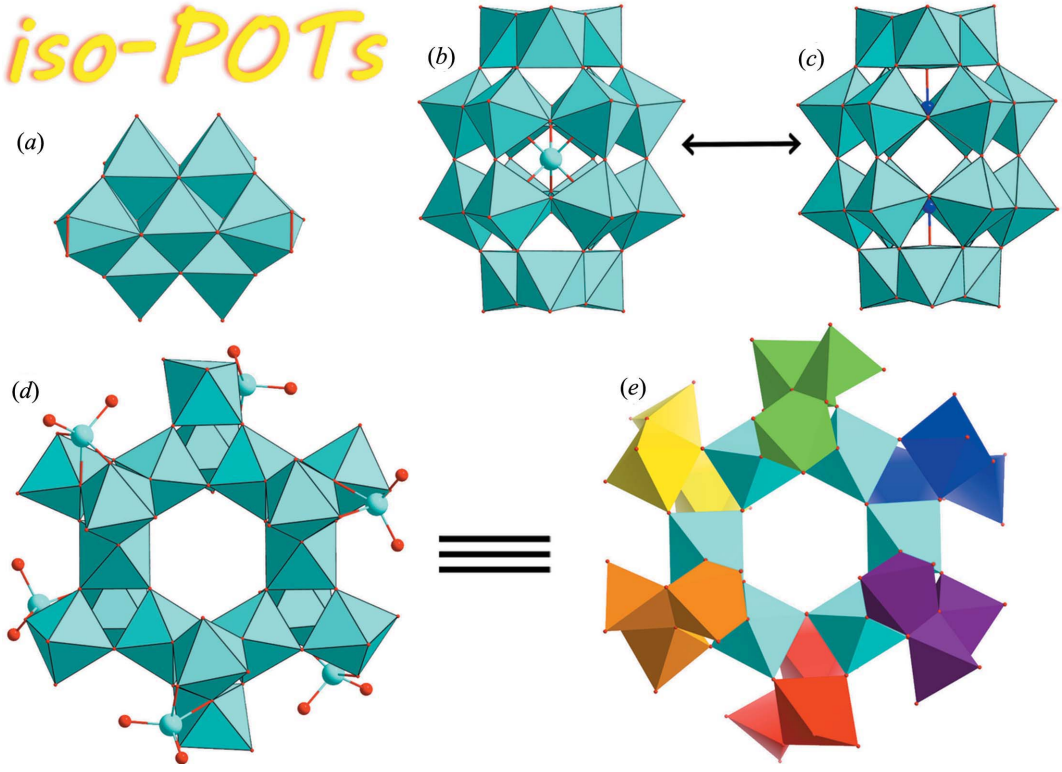

Figure 3
(*a*) The diperoxoheptatungstate $[W_7O_{22}(O_2)_2]^{6-}$. (*b*) The Dawson-like iso-POT $[H_4W^{VI}{}_{19}O_{62}]^{6-}$. (*c*) The Dawson-type phosphotungstate $[W_{18}O_{54}(PO_4)_2]^{6-}$. (*d*) The structure of iso-POT $[W_{24}O_{84}]^{24-}$ with six WO_5 units. (*e*) The inner ring formed by six vertex-sharing WO_6 octahedra and the six W_3O_{13} units, shown with different colours, in the $[W_{24}O_{84}]^{24-}$ cluster. Colour key: WO_6 blue, O red and P dark blue.

discovered three IPTMDs, namely, chain-like $[H_4CoW_{11}O_{39}]^{6-}$, cobalt-trapped $[H_4CoW_{22}O_{76}(H_2O)_2]^{14-}$ and saddle-shaped $[H_{16}Co_8W_{200}O_{660}(H_2O)_{40}]^{88-}$ (Oliva *et al.*, 2012). After the integration of compositional and time-dependent space, such a networked reactor system is transformative for the rapid screening of a large number of self-assembly reactions and allows the systematic combination of one-pot reactions of similar systems as a function of time or composition permitting the exploration of virtual libraries of building blocks. To a great extent the use of the above mentioned flexible one-pot reaction strategy accelerates the discovery of new types of iso-POT-based crystalline materials.

Apart from the one-pot reaction strategy, a stepwise synthetic strategy or a so-called step-by-step reaction strategy with a high level of controllability has also been developed. Under this strategy, preformed iso-POTs, metal clusters or metal complexes are used as templates and induce the fabrication of large iso-POT aggregations or unexpected iso-POT-based transition-metal (organometal) derivatives, or IPTM(OM)Ds. In detail, the stepwise assembly mainly includes three synthetic routes: (i) reaction of preformed iso-POT precursors with other reagents (namely, organic ligands, TM cations, RE cations and counter-cations) (Chi *et al.*, 2014; Han *et al.*, 2014; Liu *et al.*, 2006; Li *et al.*, 2002; Pang *et al.*, 2008); (ii) introduction of one type of prefabricated mononuclear metal complex or polynuclear metal cluster into the simple tungstate system (Bi *et al.*, 2004; Fang & Luban, 2011; Meng *et al.*, 2013); (iii) combination of the preformed iso-POT precursors and the preformed mononuclear metal complexes (Han *et al.*, 2001). Here, some typical stable and metastable iso-POT precursors can be listed as follows: (i) the Lindqvist hexatungstate $[W_6O_{19}]^{2-}$; (ii) the planar heptatungstate $[W_7O_{24}]^{6-}$ (Hartl *et al.*, 1993); (iii) the decatungstate $[W_{10}O_{32}]^{4-}$ with D_{4h} symmetry (Liu *et al.*, 2006); (iv) the paradodecatungstate $[H_2W_{12}O_{42}]^{10-}$; (v) the Keggin-type metadodecatungstate $[H_2W_{12}O_{40}]^{6-}$ (Sprangers *et al.*, 2006). Notably, these above-mentioned iso-POT precursors can self-decompose and reassemble into their derivative fragments, which provides numerous opportunities for synthesizing multifunctional iso-POT-based materials. For instance, under hydrothermal conditions, the one-dimensional (1D) chain-like chiral compound $[Cu_3(L)_3(H_2O)_2(H_2W_{12}O_{40})]\cdot 4H_2O$ {*L* = 2-[4,6-bis(pyridin-2-yl)pyridin-2-yl]pyridine} was prepared and spontaneously resolved by Hu and co-workers when heptatungstate $[W_7O_{24}]^{6-}$, paratungstate $[H_2W_{12}O_{42}]^{10-}$ or decatungstate $[W_{10}O_{32}]^{4-}$ was used as the starting material (Chi *et al.*, 2014). In addition, the stepwise method can be used for the synthesis of high-nuclear cluster compounds. For example, the tetradecamanganese magnetic cluster $[Mn_{14}W_{48}O_{192}H_{20}]^{26-}$ (Fang & Luban, 2011) is assembled from the red–black $[Mn_{12}(CH_3COO)_{16}(H_2O)_4O_{12}]$ (Lis, 1980). Moreover, the stepwise synthetic strategy can induce the formation of

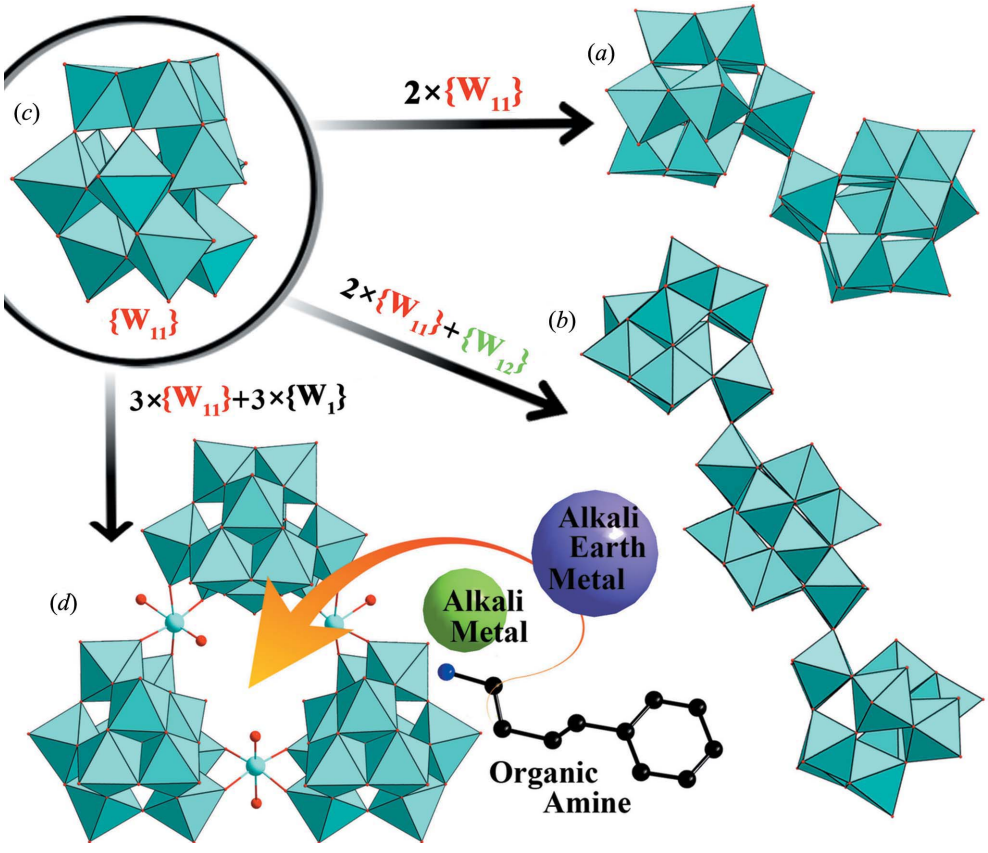

Figure 4
(*a*) The S-shaped $[H_4W_{22}O_{74}]^{12-}$ cluster. (*b*) The '§'-shaped $[H_{10}W_{34}O_{116}]^{18-}$ cluster. (*c*) The structure of the $[W_{11}O_{38}]^{10-}$ half-unit. (*d*) The threefold-symmetric Celtic ring-like $[H_4W_{36}O_{120}]^{12-}$ cluster. Colour key: WO_6 blue, O red, C black and N dark blue.

extended three-dimensional (3D) porous frameworks. In 2008, Chen used $[H_2W_{12}O_{40}]^{6-}$ as the precursor to combine with Ag^+ and Ce^{3+} linkers to form a purely inorganic 3D framework with two kinds of channels (Pang *et al.*, 2008).

Hitherto, the synthetic strategies used for the construction of iso-POTs and their derivatives can be mainly divided into four types: (i) conventional solution synthesis with simple initial materials; (ii) conventional solution synthesis with preformed iso-POT precursors, TM clusters or metal complexes; (iii) the hydro(solvo)thermal method with simple initial materials; (iv) the hydro(solvo)thermal method with preformed iso-POT precursors. We believe that many more reaction types will be found with the development of the iso-POT field. It can also be expected that further modulation of the synthetic strategies will have great potential for the creation of novel iso-POT-based crystalline materials with promising applications by introducing different functional groups.

3. Representative structure types of iso-POMs and their functional derivatives

The development and improvement of synthetic strategies contribute greatly to the structural diversity of iso-POT-based crystalline materials. Up to now, the family of iso-POT-based crystalline materials has been expanded to more than 100 compounds. Thus, there is an urgent demand for a general classification scheme in consideration of the diverse and complex structural features of iso-POT-based crystalline materials. In a critical review reported by Cronin, great stress is laid on the synthetic strategy of introducing organocations into a tungstate system to fabricate novel iso-POTs (Long *et al.*, 2007). In their subsequent review, they also systematically classified the structures of iso-POTs into several types in terms of their basal building blocks (Long *et al.*, 2010). Following these two reviews and based on recent growth in this field, here, we not only summarize the structure types of iso-POTs, but also provide an up-to-date progress report of their functional derivatives modified by various metal ions. Meanwhile, among them, some representative iso-POT-based crystalline materials from low to high nuclearity will be exclusively listed in a table to give readers a systematic and comprehensive view (Table 1).

3.1. The progress on iso-POTs

In the early stage of iso-POT chemistry, a series of examples, such as $[W_4O_8(O_2)_6(CO_3)]^{6-}$ (Stomberg, 1985), $[W_5O_{19}]^{8-}$ (Fuchs *et al.*, 1996), $[W_6O_{19}]^{2-}$ (Bhattacharyya *et al.*, 1989; Li *et al.*, 2002), $[HW_6O_{21}]^{5-}$, $[H_3W_6O_{22}]^{5-}$ (Hartl *et al.*, 1993), $[\{H(SO_4)W_3O_7(O_2)_2\}_2O]^{4-}$ (Hashimoto *et al.*, 1991), $[W_7O_{24}]^{6-}$ (Fuchs & Flindt, 1979), $[W_{11}O_{38}]^{10-}$ (Lehmann & Fuchs, 1988) and $[H_2W_{12}O_{42}]^{10-}$ (Allmann, 1971), were synthesized by addition and condensation reactions in aqueous tungstate solution. It has been proven that iso-POT structure types are formed depending primarily on the degree of acidification of the tungstate solution. As these examples have been exclusively listed in other articles, we herein only focus on those published subsequently.

In 2004, Suzuki *et al.* determined the novel diperoxo-isopolytungstate $[W_7O_{22}(O_2)_2]^{6-}$ by dissolving tungsten powder in hydrogen peroxide solution (Fig. 3*a*) (Suzuki *et al.*, 2004). Such an anion has a Lindqvist-type heptametalate structure, in which the metal atoms are located in a bent 2–3–2 arrangement with the central W_3 section as the hinge and the two peroxo groups coordinate to the W atoms at both ends of the W_3 section. By means of using the large and flexible protonated triethanolamine as the organic counter-cation, Cronin and co-workers synthesized a new type of iso-POT, $[H_4W^{VI}_{19}O_{62}]^{6-}$, by refluxing a solution of sodium tungstate and triethanolamine (TEA) for more than 3 d at pH 0.8 and showed a Dawson-type $\{W_{18}\}$ cage {for instance, $[W_{18}O_{54}(PO_4)_2]^{6-}$} featuring an additional W centre located at the centre of the Dawson-type cluster after removing two heteroatoms (Long, Kögerler *et al.*, 2006) (Figs. 3*b* and 3*c*). As far as we know, the novel iso-POT $[H_4W_{19}O_{62}]^{6-}$ represents the first example of an isopolyanion with a Dawson-type polyoxoanion skeleton. Interestingly, in this work, only the above-mentioned iso-POT $[W_{10}O_{32}]^{4-}$ anion can be obtained in the absence of bulky $TEAH^+$ organic cations, which indicates the existence of a crucial cation effect. Furthermore, the iso-POT $[W_{24}O_{84}]^{24-}$ anion was obtained by Hartl *et al.* with the participation of Cs^+ ions (Brüdgam *et al.*, 1998) (Fig. 3*d*). This ring-like iso-POT is made up of six vertex-sharing WO_6 octahedra and six W_3O_{13} groups, in which six vertex-sharing WO_6 octahedra form an inner ring and six W_3O_{13} groups are condensed to this ring *via* common octahedral vertices (Fig. 3*e*). It is worth noting that not only is it made up of WO_6 octahedra, but it also includes WO_5 subunits, which is very rare in the area of iso-POTs. Subsequently, Cronin *et al.* once again isolated two novel iso-POT cluster architectures by employing a combination of pH and anion control, namely, the S-shaped $[H_4W_{22}O_{74}]^{12-}$ ($\{W_{22}\}$) cluster (Fig. 4*a*) and the related §-shaped $[H_{10}W_{34}O_{116}]^{18-}$ ($\{W_{34}\}$) cluster (Fig. 4*b*) (Miras *et al.*, 2008). The S-shaped $\{W_{22}\}$ cluster is obtained in aqueous solution with a pH of 3.4, and can be considered to be formed by the fusion of two $[W_{11}O_{38}]^{10-}$ ($\{W_{11}\}$) half-units (Fig. 4*c*) in a staggered fashion by the sharing of two μ_2-O atoms. When the pH was adjusted to about 2.4, the rod-shaped crystals of the $\{W_{34}\}$ cluster can be isolated, which can be described as an additional paradodecatungstate $[H_2W_{12}O_{42}]^{10-}$ connecting the two $\{W_{11}\}$ units leading to the trilaminar §-shaped $[H_{10}W_{34}O_{116}]^{18-}$cluster. Thus, such a structural evolution from a $\{W_{22}\}$ to a $\{W_{34}\}$ cluster demonstrates that the structures of iso-POTs are more flexible and diverse. Furthermore, based upon the linkage of $\{W_{11}\}$ building blocks, Cronin's group simultaneously addressed a threefold-symmetric Celtic ring-like iso-POT, $[H_4W_{36}O_{120}]^{12-}$, which comprises three '*cis*-edge-shared' $\{W_{11}\}$ units linked by three $\{W_1\}$ building blocks. Interestingly, the centre of this triangular cluster has a metal–oxo framework that resembles the 18-crown-6 ether structure and also exhibits the main features of crown ethers, such as the ability to incorporate different metal ions in the central cavity of the cluster. In 2005, a series of

complexes of the type $\{M\subset W_{36}\}$ ($M = K^+$, Rb^+, Cs^+, NH^{4+}, Sr^{2+} and Ba^{2+}) based on the $\{W_{36}\}$ cluster were isolated by implanting ammonium ions, alkali metal ions and alkaline earth metal ions into the cavity (Fig. 4*d*) (Long, Brücher *et al.*, 2006). Then, they further improved this assembly strategy by employing protonated amines as guests in triangular $\{W_{36}\}$ clusters and successfully isolated four hybrid organic–inorganic host–guest systems, namely, $\{[Ph(C_2H_4)NH_3]\subset[H_{12}W_{36}O_{120}]\}^{11-}$, $\{[Ph(C_4H_8)NH_3]\subset[H_{12}W_{36}O_{120}]\}^{11-}$, $\{[p(CH_2NH_3)_2C_6H_4]\subset[H_{12}W_{36}O_{120}]\}^{11-}$ and $\{[H_3N(C_6H_{12})NH_3]\subset[H_{12}W_{36}O_{120}]\}^{10-}$ (Streb *et al.*, 2008). By single-crystal X-ray diffraction and bond valence sum calculations, they comparatively investigated the supramolecular effects of the central guest amine cations and studied their structure-directing effects on the spatial arrangement stemming from the location of the protonated amine cations in the cavity of the triangular $\{W_{36}\}$ cluster. For instance, the bifunctional guest hexane-1,6-diammonium cation, with secondary amine binding sites, can act as an excellent molecular connector and directly links to two $\{W_{36}\}$ anions through electrostatic and hydrogen-bonding interactions, thus leading to supramolecular assembly in a tilted arrangement. Inspired by this innovative work, five novel supramolecular assemblies, namely $\{[C_8H_{16}(NH_3)_2]\subset[H_{12}W_{36}O_{120}]\}^{10-}$, $\{[C_9H_{18}(NH_3)_2]\subset$ cation$[H_{12}W_{36}O_{120}]\}^{10-}$, $\{[C_{10}H_{20}(NH_3)_2]\subset[H_{12}W_{36}O_{120}]\}^{10-}$, $\{[C_{12}H_{24}(NH_3)_2]_{0.5}\subset[H_{12}W_{36}O_{120}]\}^{11-}$ and $\{[(C_6H_{12})_2NH_2(NH_3)_2]\subset[H_{12}W_{36}O_{120}]\}^{11-}$, with infinite one-dimensional (1D) zigzag chains, triangular superstructures and dimeric dumb-bell-shaped units have been isolated and characterized using long-chain guest alkyldiammonium cations with various lengths, which not only indicates that systematic variation of the alkyl-chain length of the guest molecules can be utilized as a highly effective structure directing tool, but also reveals a new approach to the control of the supramolecular assembly of 'hard' metal oxides clusters using 'soft' long-chain amines. Moreover, by treating WO_4^{2-} with dimethylamine hydrochloride in acidic aqueous medium at 277 K, Cronin *et al.* reported an approach for constructing molecular tungsten-oxide-based pentagonal building blocks $\{W(W_x)\}$ (x = 4 or 5) in a novel $[W_{21}O_{72}]^{18-}$ ($\{W_{21}\}$) unit (Fig. 5*a*) and exhibited how

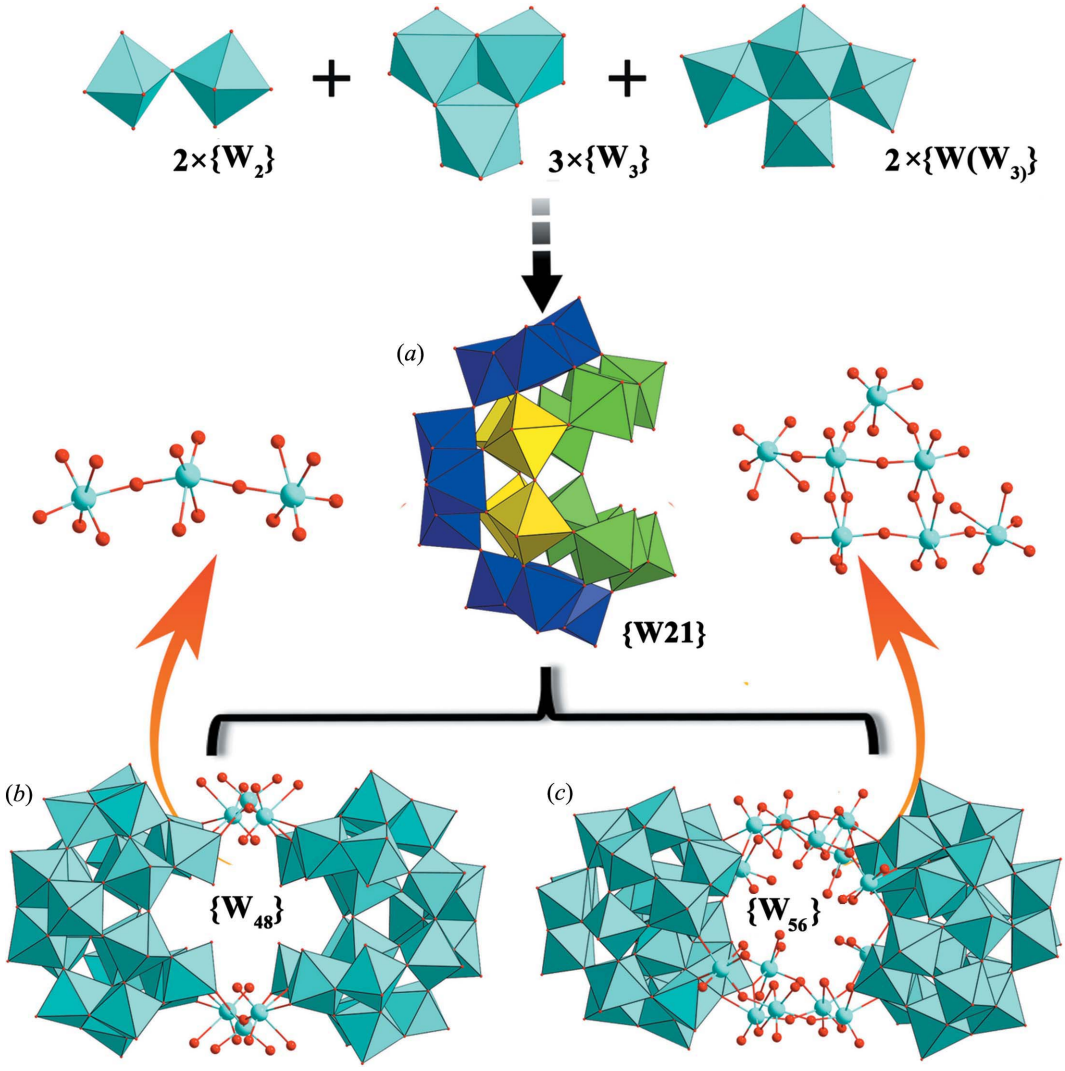

Figure 5
(*a*) The novel $[W_{21}O_{72}]^{18-}$ cluster. (*b*) The dimeric $[H_{12}W_{48}O_{164}]^{28-}$ cluster. (*c*) The dimeric $[H_{20}W_{56}O_{190}]^{24-}$ cluster. Colour key: WO_6 blue and O red.

these building blocks lead to two gigantic molecular architectures, *i.e.* $[H_{12}W_{48}O_{164}]^{28-}$ ($\{W_{48}\}$) (Fig. 5*b*) and $[H_{20}W_{56}O_{190}]^{24-}$ ($\{W_{56}\}$) (Fig. 5*c*), which represent the largest iso-POTs to date. In the former, the overall nano-sized cluster has C_{2h} symmetry, with the C_2 axis passing through the central $\{W_1\}$ units, and comprises two $\{W_{21}\}$ building blocks connected together in a parallel double-stranded fashion with dimensions of 4.3 nm in length and 1.4 nm in width. Under a similar reaction of the $\{W_{48}\}$ cluster at a higher pH of 2.0 in the presence of $Te(OH)_6$, the expanded package of the $\{W_{56}\}$ cluster was isolated. Unlike the former, the two $\{W_{21}\}$ building blocks are twisted at an angle of 62.2°, creating a central double-stranded motif with the racemate space group $P\overline{1}$. It is also worth noting that $\{W_{56}\}$ is the first example of a molecular metal oxide cluster with a chiral 'double-stranded' motif (Zhan *et al.*, 2015).

3.2. The progress on IPTMDs

In the past decade, a library of inorganic and organic–inorganic hybrid IPTMDs with monomeric to polymeric structures has been discovered through hydrothermal treatment or the conventional aqueous method. For instance, with a mixture of Cu^{2+}, 2,2′-bipyridine and WO_4^{2-} in acidic aqueous conditions, Zubieta and co-workers synthesized a dimeric monovacant Lindqvist-type IPTMD [{Cu(2,2′-bipyridine)$_2$}$_2$$W_{10}O_{32}$]·$2H_2O$ (Fig. 6*a*), featuring two [Cu(2,2′-bipyridine)$_2$]$^{2+}$ subunits linked to the decatungstate $[W_{10}O_{32}]^{4-}$ through terminal O atoms (Devi *et al.*, 2003). Subsequently, another inorganic–organic hybrid decatungstate, $[Cu_2(L1)_2Cl_2]_2(W_{10}O_{32})]$ ($L1$ = terpyridine), was obtained by Hu *et al.* through reaction of $Cu(CH_3COO)_2{\cdot}H_2O$, the ligand and the prefabricated iso-POT precursor ($[H_2W_{12}O_{40}]^{6-}$) under hydrothermal conditions (Fig. 6*b*), which successfully proves the decomposition and reassembly of $[H_2W_{12}O_{40}]^{6-}$ leading to the formation of $[W_{10}O_{32}]^{4-}$ in aqueous solution. In this compound, the two copper centres are bridged by one μ_2-Cl ligand to form a dinuclear cluster and are linked to the decatungstate to form a polynuclear structure, which is not common in POM chemistry (Chi *et al.*, 2014). In 2012, Cronin *et al.* discovered the mono-Co-incorporated IPTMD $[H_4CoW_{11}O_{39}]^{6-}$ (Oliva *et al.*, 2012) (Fig. 6*c*).

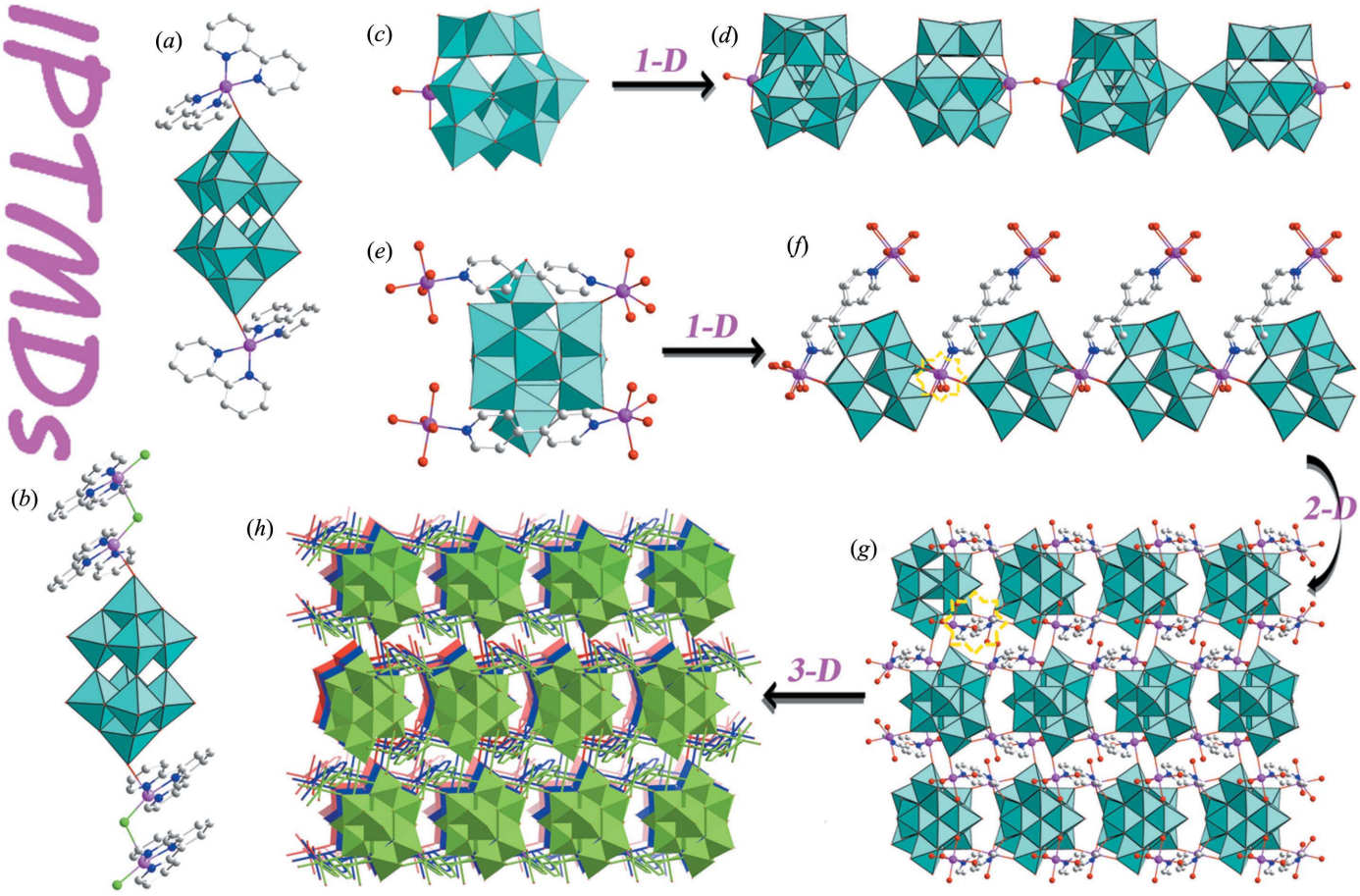

Figure 6
(*a*) The dimeric IPTMD [{Cu(2,2′-bipyridine)$_2$}$_2$$W_{10}O_{32}$]·$2H_2O$. (*b*) The decatungstate $[Cu_2(L1)_2Cl_2]_2(W_{10}O_{32})]$. (*c*) The mono-Co-substituted IPTMD $[H_4CoW_{11}O_{39}]^{6-}$. (*d*) The 1D infinite inorganic chain of $[H_4CoW_{11}O_{39}]^{6-}$. (*e*) The structure of $\{[Cu_2(bpy)(H_2O)_{5.5}]_2[H_2W_{11}O_{38}]{\cdot}3H_2O{\cdot}0.5CH_3CN\}$. (*f*) The 1D chain of $\{[Cu_2(bpy)(H_2O)_{5.5}]_2[H_2W_{11}O_{38}]\}$. (*g*) The 2D sheet structure of $[Cu_2(bpy)(H_2O)_{5.5}]_2[H_2W_{11}O_{38}]{\cdot}3H_2O{\cdot}0.5CH_3CN$. (*h*) The 3D metal–organic framework constructed from $[Cu_2(bpy)(H_2O)_{5.5}]_2[H_2W_{11}O_{38}]{\cdot}3H_2O{\cdot}0.5CH_3CN$ units. Colour key: WO_6 blue, O red, TM pink, C grey and N dark blue.

It is interesting to note that the disordered Co^{2+} cations act as bridges linking neighbouring iso-POT fragments through a Co—O—W linkage, leading to a 1D infinite inorganic chain (Fig. 6*d*). What is more, in 2014, Han *et al.* also synthesized an iso-POT-based metal–organic framework, $[Cu_2(bpy)(H_2O)_{5.5}]_2[H_2W_{11}O_{38}]\cdot 3H_2O\cdot 0.5CH_3CN$, based on the $[H_2W_{11}O_{38}]^{8-}$ ($\{W_{11}\}$) cluster under solvothermal conditions (Fig. 6*e*) (Han *et al.*, 2014). In this compound, two $\{W_{11}\}$ clusters are alternately connected by two $[Cu_2(bpy)(H_2O)_{5.5}]^{4+}$ cations in the end-to-end fashion and result in a 1D chain (Fig. 6*f*). Adjacent 1D chains are then linked *via* Cu1—bpy—Cu2 units in an opposite direction forming a 2D wave-like sheet in the *ab* plane (Fig. 6*g*). Such 2D sheets are further stacked in a parallel manner, leading to 1D channels, with the copper(II) cations aligned in the channels (Fig. 6*h*). This iso-POT-based metal–organic framework has been successfully applied to improve the cyanosilylation of aldehydes with excellent conversion efficiency by a heterogeneous reaction (Table 2), which may be attributed to the suitable distribution of copper(II) and $\{W_{11}\}$ in the framework providing effective contacts with substrates at the same time (Han *et al.*, 2014). Besides, the paradodecatungstate cluster $[H_2W_{12}O_{42}]^{10-}$ has also been selected as an ideal primary building block for the construction of extended IPTMDs (Fig. 7*a*). In 2008, one copper-based IPTMD, $[Cu(H_2O)_2(H_2W_{12}O_{42})]^{8-}$ (Fig. 7*b*), and two cadmium-based IPTMDs,

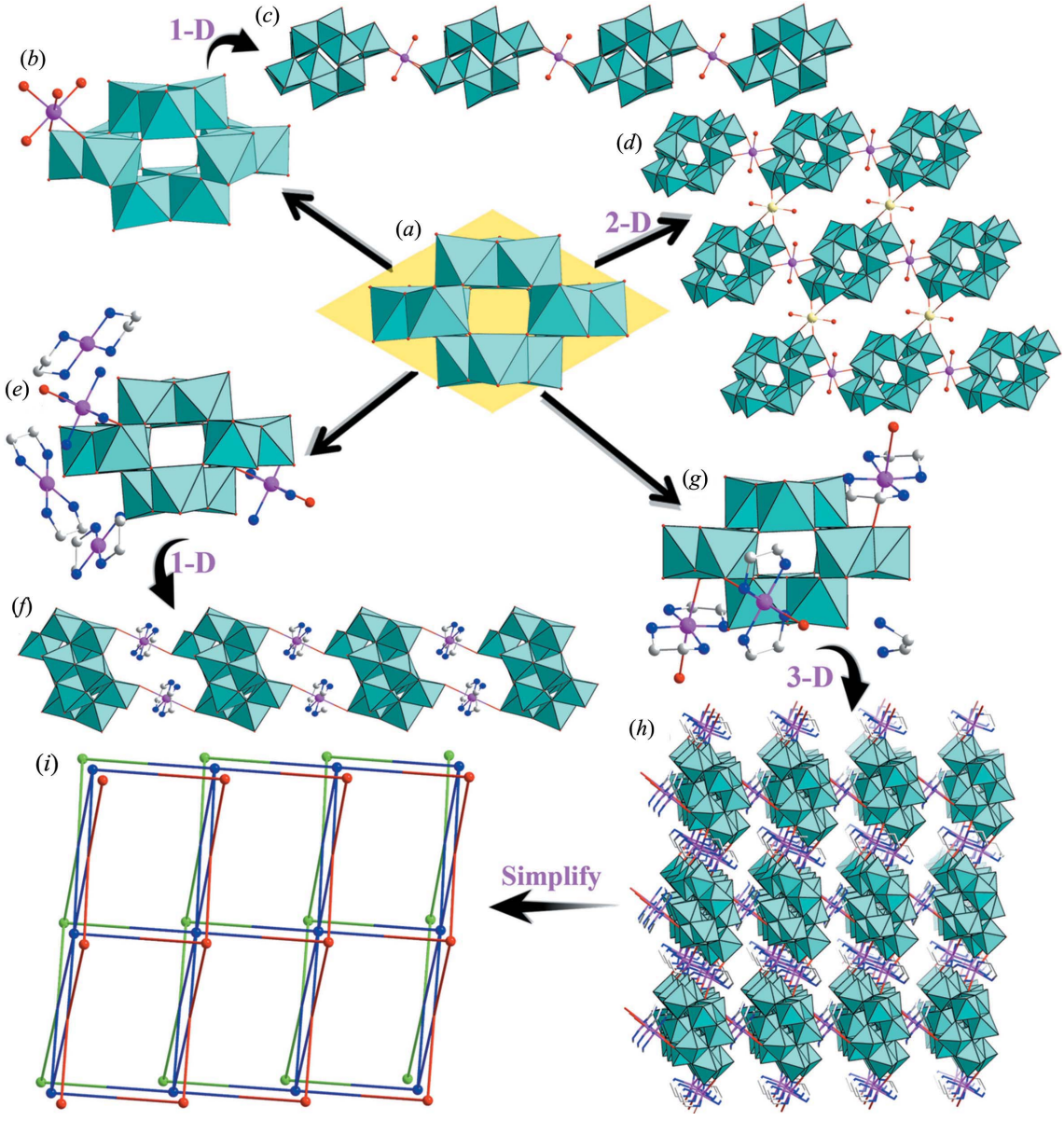

Figure 7
(*a*) The paradodecatungstate cluster $[H_2W_{12}O_{42}]^{10-}$. (*b*) The structure of IPTMD $[Cu(H_2O)_2(H_2W_{12}O_{42})]^{8-}$ or $[Cd(H_2O)_2(H_2W_{12}O_{42})]^{8-}$. (*c*) The 1D chain of $[Cu(H_2O)_2(H_2W_{12}O_{42})]^{8-}$ or $[Cd(H_2O)_2(H_2W_{12}O_{42})]^{8-}$. (*d*) The 2D framework of $[Cd_{1.3}(H_2O)_2(H_2W_{12}O_{42})]^{7.4-}$. (*e*) The organic–inorganic hybrid IPTMD $[Cu(en)_2]_3[\{Cu(en)_2\}_2(H_2W_{12}O_{42})]\cdot 12H_2O$. (*f*) The 1D chain of $[Cu(en)_2]_3[\{Cu(en)_2\}_2(H_2W_{12}O_{42})]\cdot 12H_2O$. (*g*) The Cu-substituted IPTMD $(enH_2)_2[Cu(en)_2]_3[H_2W_{12}O_{42}]\cdot 6H_2O$. (*h*) The 3D open-framework of $(enH_2)_2[Cu(en)_2]_3[H_2W_{12}O_{42}]\cdot 6H_2O$. (*i*) The simplified 3D open-framework of $(enH_2)_2[Cu(en)_2]_3[H_2W_{12}O_{42}]\cdot 6H_2O$. Colour key: WO_6 blue, O red, TM pink, C grey and N dark blue.

$[Cd(H_2O)_2(H_2W_{12}O_{42})]^{8-}$ and $[Cd_{1.3}(H_2O)_2(H_2W_{12}O_{42})]^{7.4-}$, were synthesized and characterized by Wu and co-workers (Li, Bi *et al.*, 2008). Both $[Cu(H_2O)_2(H_2W_{12}O_{42})]^{8-}$ and $[Cd(H_2O)_2(H_2W_{12}O_{42})]^{8-}$ display analogous 1D structures with two adjacent paradodecatungstate clusters linked by $[Cu(H_2O)_2]^{2+}$ or $[Cd(H_2O)_2]^{2+}$ units (Fig. 7*c*), while in the structure of $[Cd_{1.3}(H_2O)_2(H_2W_{12}O_{42})]^{7.4-}$, each $[H_2W_{12}O_{42}]^{10-}$ cluster acts as a multidentate ligand and coordinates to Cd^{2+} ions through the terminal O atoms, leading to an infinite 2D framework (Fig. 7*d*). The electrochemical behaviours of $[Cu(H_2O)_2(H_2W_{12}O_{42})]^{8-}$ and $[Cd_{1.3}(H_2O)_2(H_2W_{12}O_{42})]^{7.4-}$ were studied by CV measurements and the results display a successive W-centred reduction process, and both of them also exhibit excellent electrocatalytic activity towards the reduction of NO_2^-. Besides, by the reaction of Cu^{2+}, WO_4^{2-}, ethylenediamine and H_2O under hydrothermal conditions for 72 h, Lin *et al.* acquired the chain-like IPTMD $[Cu(en)_2]_3[\{Cu(en)_2\}_2(H_2W_{12}O_{42})]\cdot 12H_2O$ (Fig. 7*e*), where the paradodecatungstate $[H_2W_{12}O_{42}]^{10-}$ units are interconnected by bridging $[Cu(en)_2]^{2+}$ groups into a 1D chain structure (Fig. 7*f*). This compound was used as the catalyst in the photooxidation of cyclohexane yielding an overall oxidative conversion of 36% of cyclohexane (Lin *et al.*, 2003). Subsequently, our group also obtained an organic–inorganic hybrid paratungstate derivative, *i.e.* $(enH_2)_2[Cu(en)_2]_3[H_2W_{12}O_{42}]\cdot 6H_2O$ in 2012 (Fig. 7*g*) (Li *et al.*, 2012). In this structure, each paradodeca-

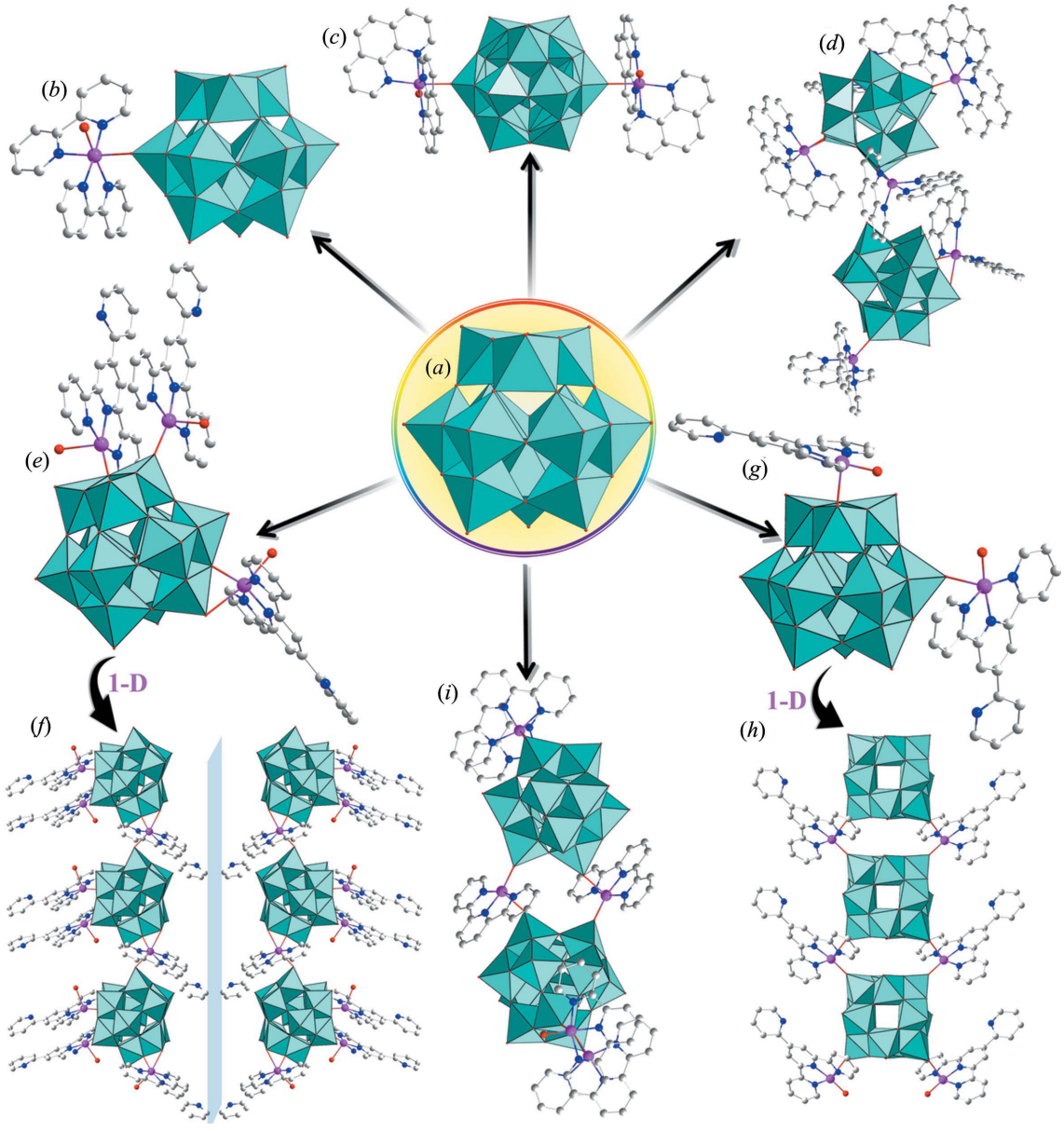

Figure 8
(*a*) The metadodecatungstate cluster $[H_2W_{12}O_{40}]^{6-}$. (*b*) The structure of IPTMD $[Ni(bpy)_3]_{1.5}[Ni(bpy)_2(H_2O)\{H_3W_{12}O_{40}\}]\cdot 0.5H_2O$. (*c*) The structure of IPTMD $[\{Ni(phen)_2(H_2O)\}_2\{H_4W_{12}O_{40}\}]\cdot 4H_2O$. (*d*) The structure of IPTMD $[\{Cu(phen)_2\}_4\{H_2W_{12}O_{40}\}][\{Cu(phen)_2\}_2\{H_2W_{12}O_{40}\}]\cdot 3H_2O$. (*e*) The structure of IPTMD $[Cu_3(L2)_3(H_2O)_2(H_2W_{12}O_{40})]\cdot 4H_2O$. (*f*) The two enantiotopic 1D chains of $[Cu_3(L2)_3(H_2O)_2(H_2W_{12}O_{40})]\cdot 4H_2O$. (*g*) The structure of IPTMD $[CuL2]_2[H_4W_{12}O_{40}]\cdot 5H_2O$. (*h*) The 1D chain of $[CuL2][H_4W_{12}O_{40}]\cdot 5H_2O$. (*i*) The structure of IPTMD $[Cu_3(L1)_3(H_2O)(H_2W_{12}O_{40})]_2\cdot 4H_2O$. Colour key: WO_6 blue, O red, TM pink, C grey and N dark blue.

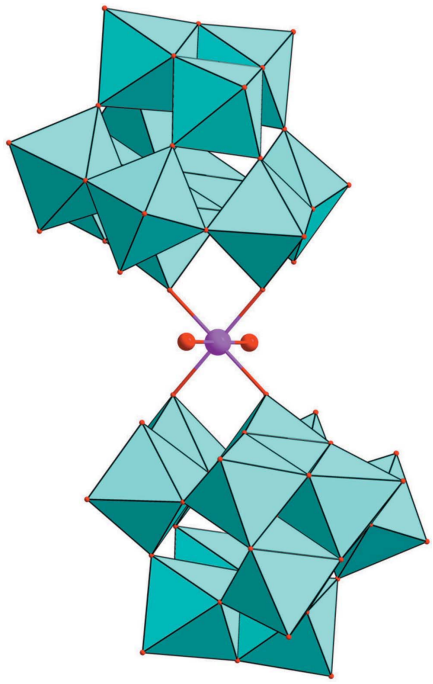

Figure 9
The dimeric cobalt-trapped IPTMD $[H_4CoW_{22}O_{76}(H_2O)_2]^{14-}$. Colour key: WO_6 blue, O red and Co pink.

tungstate $[H_2W_{12}O_{42}]^{10-}$ subunit acts as a hexadentate ligand and bonds to six Cu^{2+}cations leading to a 3D organic–inorganic hybrid architecture with a Schläfli symbol of $4^{12}6^3$ (Figs. 7*h* and 7*i*). Notably, this represents the first 6-connected 3D open framework constructed from paradodecatungstate clusters in POM chemistry. Apart from the paradodecatungstate cluster $[H_2W_{12}O_{42}]^{10-}$, the metadodecatungstate cluster $[H_2W_{12}O_{40}]^{6-}$ has also been employed as an ideal starting point for the construction of novel IPTMDs (Fig. 8*a*). Typically, Zubieta and co-workers isolated three novel TM-complex-modified IPTMDs, *i.e.* $[Ni(bpy)_3]_{1.5}[Ni(bpy)_2(H_2O)\{H_3W_{12}O_{40}\}]\cdot0.5H_2O$, $[\{Ni(phen)_2(H_2O)\}_2\{H_4W_{12}O_{40}\}]\cdot4H_2O$ and $[\{Cu(phen)_2\}_4\{H_2W_{12}O_{40}\}][\{Cu(phen)_2\}_2\{H_2W_{12}O_{40}\}]\cdot3H_2O$, under hydrothermal conditions (Figs. 8*b*, 8*c* and 8*d*) (Devi *et al.*, 2003). Recently, two enantiotopic 1D chain compounds, *i.e.* $[Cu_3(L2)_3(H_2O)_2(H_2W_{12}O_{40})]\cdot4H_2O$ {*L*2 = 2-[4,6-bis(pyridin-2-yl)pyridin-2-yl]-pyridine}, with chiral space group $P2_12_12_1$, were synthesized by Hu and co-workers with a lack of any chiral auxiliary (Chi *et al.*, 2014). The asymmetric unit in this compound is built by one metadodecatungstate $[H_2W_{12}O_{40}]^{6-}$ clusters, two $[CuL2(H_2O)]^{2+}$ units and one $[CuL2]^{2+}$ unit (Fig. 8*e*), and adjacent asymmetric units are linked together *via* $[CuL2]^{2+}$ bridges generating a 1D chain along the *a* axis (Fig. 8*f*). Noticeably, this pair of enantiomers represents the first example of spontaneously isolated chiral iso-POTs without any chiral source. Subsequently, under similar reaction conditions, another two organic–inorganic achiral IPTMDs, *i.e.* $[CuL2]_2[H_4W_{12}O_{40}]\cdot5H_2O$ and $[Cu_3(L1)_3(H_2O)(H_2W_{12}O_{40})]_2\cdot4H_2O$, were also isolated (Chi *et al.*, 2014). In the former (Fig. 8*g*), each $[H_4W_{12}O_{40}]^{4-}$ cluster acts as a quadridentate inorganic ligand that connects with four Cu^{II} centres, while each Cu^{II} centre connects two neighbouring $[H_4W_{12}O_{40}]^{4-}$ clusters to construct a 1D chain (Fig. 8*h*). The latter is composed of two enantiotopic $[Cu_3(L2)_3(H_2O)(H_2W_{12}O_{40})]$ subunits, which is induced by the metal–organic groups asymmetrically occupying two sides of the $[H_2W_{12}O_{40}]^{6-}$ cluster. As two enantiotopic subunits are connected into a dimeric structural unit, and such a linking arrangement leads to the existence of an inversion centre, thus, IPTMD $[Cu_3(L2)_3(H_2O)(H_2W_{12}O_{40})]_2\cdot\cdot4H_2O$ is mesomeric (Fig. 8*i*). Apart from the $\{W_{12}\}$-based IPTMDs, in the presence of the Co^{2+} templating ion, another dimeric cobalt-trapped IPTMD, $[H_4CoW_{22}O_{76}(H_2O)_2]^{14-}$, containing two $[W_{11}O_{38}]^{10-}$ subunits was discovered by Cronin and co-workers by a one-pot reaction (Fig. 9) (Oliva *et al.*, 2012). Moreover, the emergence of some novel high-nuclear IPTMDs has also aroused worldwide attention. In 2011, Fang *et al.* demonstrated a step-by-step approach to synthesize the tetradecamanganese magnetic cluster $[Mn_{14}W_{48}O_{192}H_{20}]^{26-}$ with two high-spin Mn_7 cores by reacting the prefabricated mixed-valence $\{Mn^{III}{}_8Mn^{IV}{}_4\}$ cluster with $WO_4{}^{2-}$ in the presence of dimethylamine hydrochloride (Figs. 10*a* and 10*b*). Different from the mixed-valence $\{Mn^{III}{}_8Mn^{IV}{}_4\}$ cluster, its magnetic behaviour manifests dominant antiferromagnetic interactions and does not exhibit single-molecule magnet behaviour, which indicates that interactions between magnetic cores and metal oxide clusters could greatly alter the magnetic behaviours in a conspicuous way (Fang & Luban, 2011). Reviewing the history, in 2015, Cronin *et al.* synthesized a gigantic nanoscale IPTMD, $[(C_2H_8N_2)_4Cu_{16}(H_{12}W_{92}O_{311})]^{26-}$, with 16 Cu^{2+} cations anchored symmetrically in its structure, which was obtained from the reaction of $WO_4{}^{2-}$ in water with copper acetate solution in the presence of ethylenediamine dihydrochloride (Fig. 10*c*). Remarkably, this $[(C_2H_8N_2)_4Cu_{16}(H_{12}W_{92}O_{311})]^{26-}$ cluster has four novel $\{W_{21}O_{72}\}$ building units that are connected in a helical fashion containing three types of pentagonal units (namely, $\{W(W_3)\}$, $\{W(W_4)\}$ and $\{W(W_5)\}$) and can be viewed as the highest-nuclear organic–inorganic IPTMD up to now (Zhan *et al.*, 2015). Moreover, by utilizing a networked reaction system, Cronin and co-workers also harvested a saddle-shaped tetragonal structure, $[H_{16}Co_8W_{200}O_{660}(H_2O)_{40}]^{88-}$ ($\{W_{200}Co_8\}$), more than 4 nm in diameter, representing the largest discrete iso-POT cluster so far (Oliva *et al.*, 2012) (Fig. 10*d*). The $\{W_{200}Co_8\}$ cluster consists of three types of novel fundamental building blocks, namely, $\{W_1\}$, $\{W_8\}$ and $\{W_9\}$. Thus, from a structural point of view, the discovery of the octacobalt-incorporated isopolyanion $[H_{16}Co_8W_{200}O_{660}(H_2O)_{40}]^{88-}$ is very important because this cluster is constructed from an unexpected tungstate building block library *via* multi-cobalt-trapping self-assembly.

3.3. The progress on IPREDs

The search for and discovery of novel IPREDs still remains an appealing branch owing to their intriguing properties in the areas of luminescence, catalysis, electrochemistry and magnetism by taking advantage of the electronic and structural features of RE ions (Li *et al.*, 2017). Historically, the first series of IPREDs with the formula $[RE(W_5O_{18})_2]^{9-}$ (RE =

La^{III}, Ce^{III}, Pr^{III}, Nd^{III}, Sm^{III}, Ho^{III}, Er^{III}, Yb^{III} and Y^{III}) was communicated by Peacock and Weakley in 1971 (Almeida Paz *et al.*, 2005; Peacock & Weakley, 1971), in which two $[W_5O_{18}]^{6-}$ fragments are linked together *via* a central RE cation located on a twofold rotation axis (Fig. 11*a*). In 2006, Chen's group discovered another organic–inorganic hybrid IPRED, $[Ce(H_2O)(DMF)_6(W_{10}O_{32})]\cdot DMF\cdot CH_3CH_2OH$, constructed from a decatungstate $[W_{10}O_{32}]^{4-}$ isopolyanion and a $[Ce(H_2O)(DMF)_6]^{4+}$ cation in the presence of an organic solvent (Liu *et al.*, 2006), which exhibits the first 1D right- and left-handed helical chains constructed by rare tetravalent cerium-linking decatungstate building blocks (Figs. 11*b* and 11*c*). In 2008, Cao and co-workers obtained a novel pentadecatungstate, $[H_6Ce_2(H_2O)Cl(W_5O_{18})_3]^{7-}$, consisting of a 15-membered WO_6 octahedra ring, as well as a dinuclear cerium(III) unit (Fig. 11*d*) (Li, Li *et al.*, 2008). The UV–Vis spectrum of this compound shows a blue photoluminescence with a maximum emission at 488 nm, which may be applied in blue-light photoactive materials. Subsequently, our group also carried out ground-breaking work in the development of IPREDs and successfully obtained a class of oxalate-connected IPREDs, $[RE_2(C_2O_4)(H_2O)_4(OH)W_4O_{16}]_2^{10-}$ (RE = Eu^{III}, Ho^{III}, Er^{III} and Tb^{III}), when only Na^+ ions are present in the reaction (Fig. 11*e*) (Zhao *et al.*, 2014), which represents the first rectangular double-oxalate-bridged tetra-RE cluster encapsulated divacant Lindqvist iso-POT hybrids. Intriguingly, when Na^+ and K^+ ions are simultaneously introduced into the reaction system (Zhao *et al.*, 2014), another series of square double-oxalate-bridged tetra-RE cluster anchored iso-POT hybrids, $[RE(C_2O_4)W_5O_{18}]_4^{20-}$ (RE = Eu^{III}, Ho^{III}, Er^{III} and Tb^{III}), are formed (Fig. 11*f*). Moreover, the solid-state luminescence properties and decay behaviours of $[Eu_2(C_2O_4)(H_2O)_4(OH)W_4O_{16}]_2^{10-}$ and $[Eu(C_2O_4)W_5O_{18}]_4^{20-}$ have been profoundly probed, showing the orange emission bands of the Eu^{3+} ions in the visible region (Fig. 12). In 2013, Niu and co-workers reported the first peroxo-containing IPREDs, $[RE_4(WO_4)(H_2O)_{16}\{W_7O_{22}(O_2)_2\}_4]^{14-}$ (RE = La^{III} and Pr^{III}), by reaction of Na_2WO_4 and RE ions in the presence of peroxide (Song *et al.*, 2013), where the central WO_4^{2-} core and four tetradentate $\{W_7O_{22}(O_2)_2\}$ fragments are bridged together by four $\{REO_9\}$ linkers. It is worth noting that two W atoms on opposite sides of the $\{W_7O_{22}(O_2)_2\}$ unit exhibit a distorted pentagonal bipyramidal coordination environment and the remaining W atoms adopt the common WO_6 octahedral geometry (Fig. 11*g*). What is more, a large number of IPREDs containing the $\{W_{11}\}$ unit have been reported. The undecatungstate $\{W_{11}\}$ unit can be considered to be derived from the classical Keggin metatungstate $[W_{12}O_{40}]^{8-}$ polyoxoanion: two corner-sharing $\{WO_6\}$ octahedra located on equatorial positions are first moved away

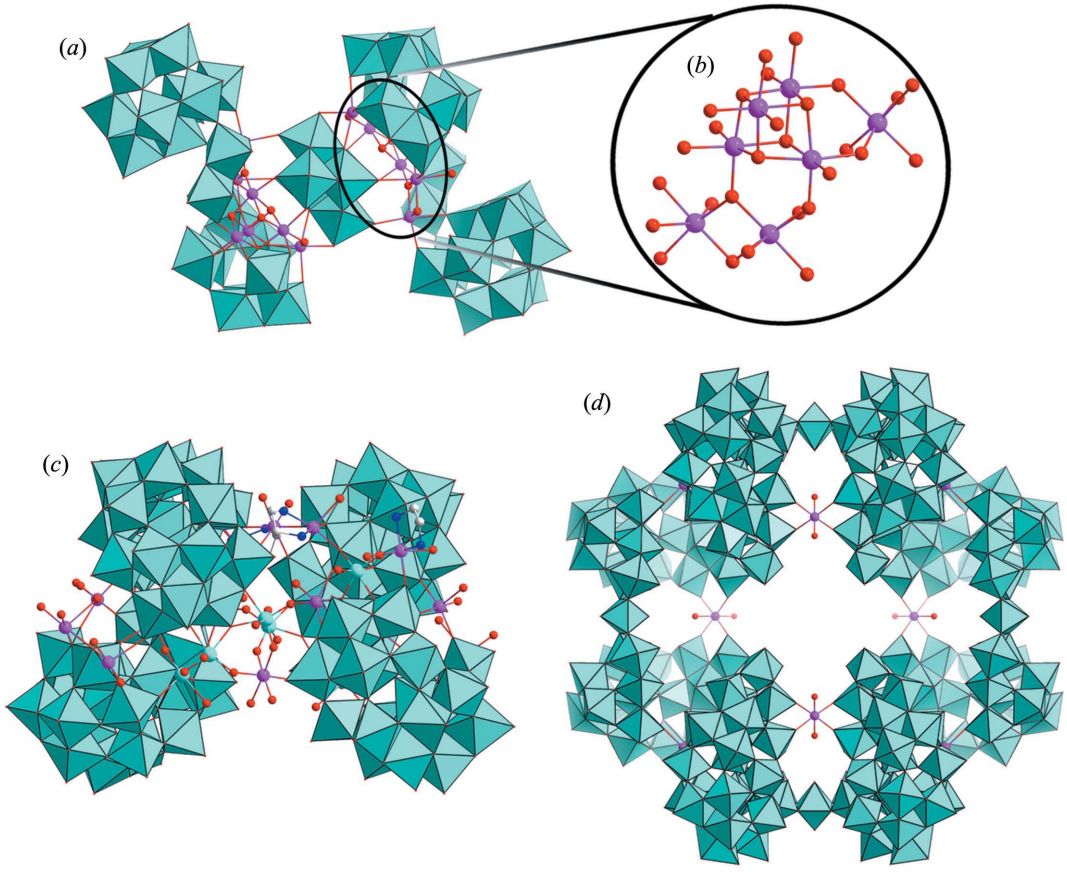

Figure 10
(*a*) The tetradecamanganese magnetic cluster $[Mn_{14}W_{48}O_{192}H_{20}]^{26-}$. (*b*) The high-spin Mn_7 core in the cluster $[Mn_{14}W_{48}O_{192}H_{20}]^{26-}$. (*c*) The gigantic nanoscale IPTMD $[(C_2H_8N_2)_4Cu_{16}(H_{12}W_{92}O_{311})]^{26-}$. (*d*) The saddle-shaped tetragonal structure $[H_{16}Co_8W_{200}O_{660}(H_2O)_{40}]^{88-}$. Colour key: WO_6 blue, O red, TM pink, C grey and N dark blue.

Table 2
Results for the catalytic cyanosilylation of aldehydes in the presence of $[Cu_2(bpy)(H_2O)_{5.5}]_2[H_2W_{11}O_{38}]\cdot 3H_2O\cdot 0.5CH_3CN$, (1)[a].

Entry	Ar	Yield (%)[b]
1	Phenyl	98.1
2	4-Methoxyphenyl	89.3
3	1-Naphthyl	87.8
4	2-Naphthyl	88.0
5	3-Formyl-1-phenylene-(3,5-di-*tert*-butylbenoate)	52.4

(*a*) Reaction conditions: $(CH_3)_3SiCN$, 1.2 mmol; aldehyde, 0.5 mmol; catalyst **1**, 0.01 mmol (2 mol%); CH_3CN, 2 ml; room tempreture under N_2 for 24 h. (*b*) The conversions were determind by ^1H NMR spectroscopy of the crude products. Reproduced with permission from Han *et al.* (2014). Copyright American Chemical Society.

from the $[W_{12}O_{40}]^{8-}$ polyoxoanion, creating the divacant Keggin $[W_{10}O_{37}]^{14-}$ segment, and then one $\{WO_6\}$ octahedron is embedded in the vacant site and grafts to two $\{W_2O_{10}\}$ groups of the $[W_{10}O_{37}]^{14-}$ segment. After that, one $\{W_3O_{13}\}$ group in the polar position of the $[W_{10}O_{37}]^{14-}$ segment rotates 60° to give rise to the unusual undecatungstate $\{W_{11}\}$ unit (Fig. 13*a*). By employing a one-pot strategy, Su's group synthesized the dicerium(III)-bridged iso-POT $[Ce_2(H_2O)_6W_{22}O_{72}(OH)_4]^{10-}$ unit at pH 5.0 (Chen, Wang *et al.*, 2014), where two $\{W_{11}\}$ subunits coordinate to two Ce^{III} centres located at the inflection point through two μ_3-oxo bridges (Fig. 13*b*). Besides, Kortz and our group also isolated the dimeric 22-iso-POTs $[RE_2(H_2O)_{10}W_{22}O_{71}(OH)_2]^{8-}$ (RE = La^{III}, Ce^{III}, Tb^{III}, Dy^{III}, Ho^{III}, Er^{III}, Tm^{III} and Yb^{III}), $\{[Eu(H_2O)_7]_2[Eu(H_2O)_5]_2[W_{22}O_{74}H_2]\}^{2-}$ and $\{[RE(H_2O)_4][RE(H_2O)_5]_2[W_{22}O_{74}H_2]\}^{5-}$ [RE = Gd^{III}, Tb^{III}, Dy^{III}, Ho^{III}, Er^{III}, Tm^{III}, Yb^{III}, Lu^{III} and Y^{III}], in which two undecatungstate $\{W_{11}\}$ units are fused by two corner-sharing W—O—W bridges generating the $[H_2W_{22}O_{74}]^{14-}$ ($\{W_{22}\}$) fragment (Ismail, Bassil *et al.*, 2009; Ismail, Dickman & Kortz, 2009; Li *et al.*, 2016, 2017). However, there are still some differences in their structures. For instance, the two RE ions in $[RE_2(H_2O)_{10}W_{22}O_{71}(OH)_2]^{8-}$ (RE = La^{III}, Ce^{III}, Tb^{III}, Dy^{III}, Ho^{III}, Er^{III}, Tm^{III} and Yb^{III}) link to neighbouring $\{W_{22}\}$ units and can further engender an overall 1D chain arrangement (Fig. 13*c*); in $\{[Eu(H_2O)_7]_2[Eu(H_2O)_5]_2[W_{22}O_{74}H_2]\}^{2-}$, the

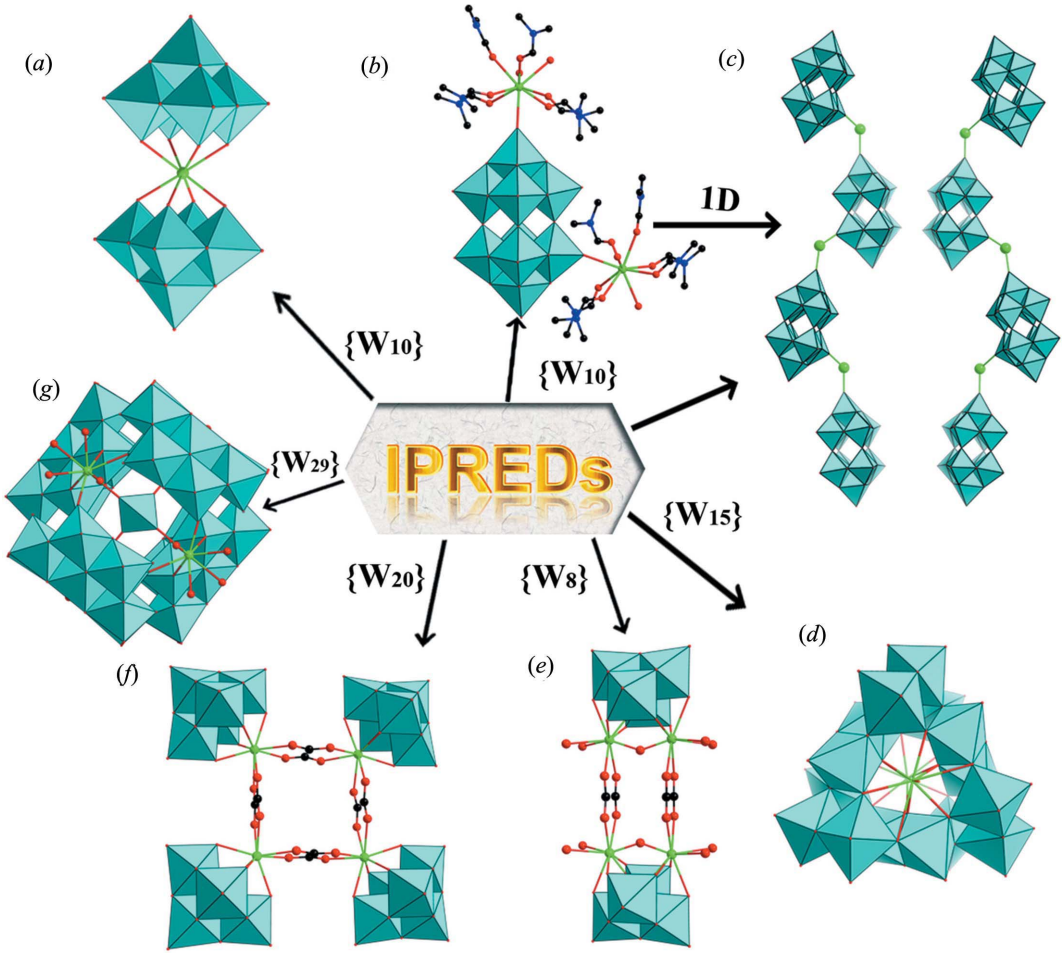

Figure 11
(*a*) The iso-10-tungstate anion $[RE(W_5O_{18})_2]^{9-}$. (*b*) The organic–inorganic hybrid IPRED $[Ce(H_2O)(DMF)_6(W_{10}O_{32})]\cdot DMF\cdot CH_3CH_2OH$. (*c*) The left- and right-handed helical chains in $[Ce(H_2O)(DMF)_6(W_{10}O_{32})]\cdot DMF\cdot CH_3CH_2OH$. (*d*) The pentadecatungstate structure of $[H_6Ce_2(H_2O)Cl(W_5O_{18})_3]^{7-}$. (*e*) The rectangular double-oxalate-bridged IPRED $[RE_2(C_2O_4)(H_2O)_4(OH)W_4O_{16}]_2^{10-}$. (*f*) The square double-oxalate-bridged IPRED $[RE(C_2O_4)W_5O_{18}]_4^{20-}$. (*g*) The peroxo-containing IPRED $[RE_4(WO_4)(H_2O)_{16}\{W_7O_{22}(O_2)_2\}_4]^{14-}$. Colour key: WO_6 blue, O red, RE green, C black and N dark blue.

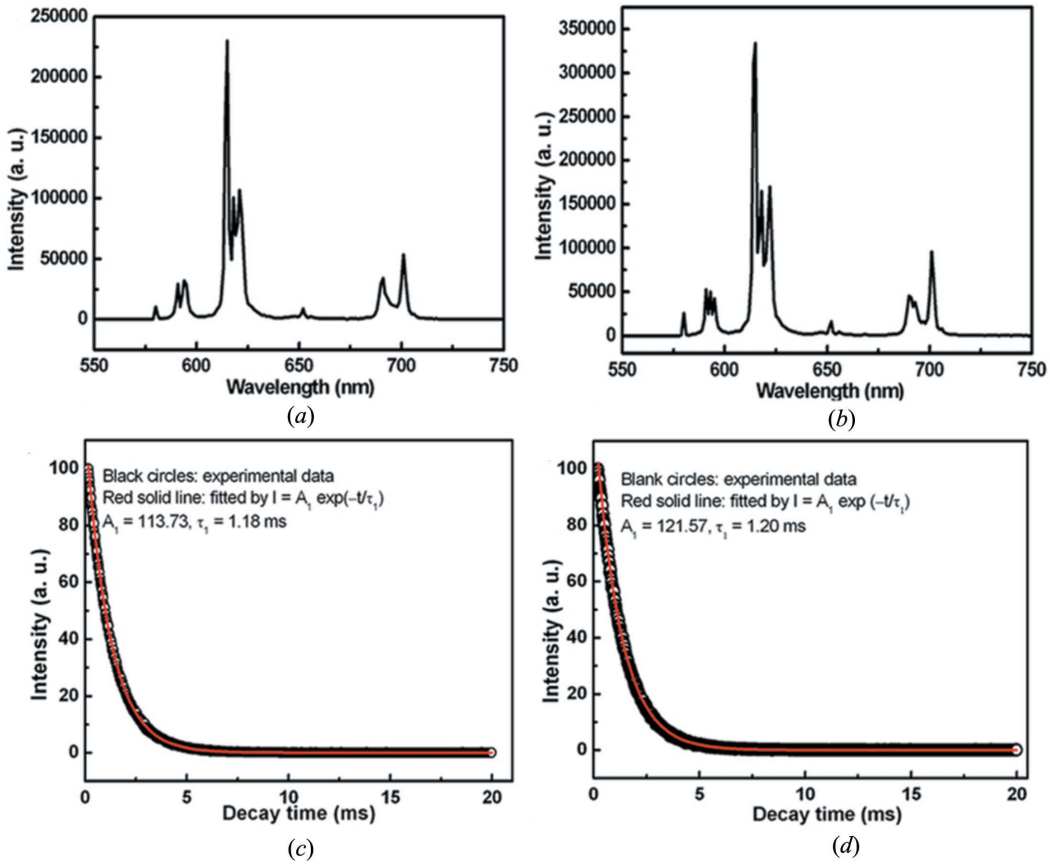

Figure 12
(*a*) The photoluminescence emission spectrum of $[Eu_2(C_2O_4)(H_2O)_4(OH)W_4O_{16}]_2^{10-}$. (*b*) The photoluminescence emission spectrum of $[Eu(C_2O_4)W_5O_{18}]_4^{20-}$. (*c*) The luminescence decay curve of $[Eu_2(C_2O_4)(H_2O)_4(OH)W_4O_{16}]_2^{10-}$. (*d*) The luminescence decay curve of $[Eu(C_2O_4)W_5O_{18}]_4^{20-}$.

$\{W_{22}\}$ units are interconnected together by four W—O—Eu1—O—W linkers, giving rise to a 1D chain motif; adjacent 1D chains are then joined through multiple W—O—Eu2—O—W connectors resulting in a 2D (4,4)-network topology (Figs. 13*d* and 13*e*). For $\{[RE(H_2O)_4][RE(H_2O)_5]_2[W_{22}O_{74}H_2]\}^{5-}$ [RE = Gd^{III}, Tb^{III}, Dy^{III}, Ho^{III}, Er^{III}, Tm^{III}, Yb^{III}, Lu^{III} and Y^{III}], since the RE2 ion is disordered over two positions with site occupancies of 50%, the molecular units are discrete and are regularly aligned in an ...*AAA*... fashion (Fig. 13*f*). Apart from the dimeric $\{W_{22}\}$ fragment, novel V-shaped $\{W_{28}\}$ units contain the $\{W_{11}\}$ unit. For example, Su *et al.* and Kortz *et al.* used the reaction of RE ions with WO_4^{2-} in aqueous acidic medium and, respectively, separated the RE-stabilized $\{W_{28}\}$ species $[Ce_2(H_2O)_{10}W_{28}O_{92}(OH)_2]^{12-}$ and $[RE_2(H_2O)_{10}W_{28}O_{93}(OH)_2]^{14-}$ (RE = Sm^{III} and Eu^{III}) (Chen, Wang *et al.*, 2014; Ismail, Bassil *et al.*, 2009; Ismail, Dickman & Kortz, 2009). Notably, the $\{W_{28}\}$ fragment consists of two kinds of building blocks, namely, two $\{W_{11}\}$ units and an extra hexatungstate $\{W_6\}$ unit (Fig. 13*g*), which is not common in POM chemistry. With further exploration, our group also addressed three intriguing hexameric IPREDs, *i.e.* $[RE_4(H_2O)_{22}W_{28}O_{94}H_2]_2^{12-}$ (RE = Pr^{III}, Nd^{III} and Sm^{III}) (Fig. 13*h*), which can be viewed as the fusion of two $\{RE_4W_{28}O_{94}\}$ subunits and which all display a 1D chain-like alignment through $[RE(H_2O)_5]^{3+}$ connectors (Li *et al.*, 2016). Furthermore, under the guidance of a pH-controlled and sulfite-anion-directed assembly strategy, Su and co-workers also obtained another two intriguing Ce^{III}-containing IPREDs, namely $[Ce_2(H_2O)_9W_{36}O_{110}(OH)_{12}]_2^{20-}$ and $[Ce_4(H_2O)_{12}W_{44}O_{144}(OH)_{12}]^{24-}$. The former consists of two identical $\{Ce_2W_{36}\}$ subunits related to each other through an inversion centre and represents the largest IPRED in POM chemistry to date (Fig. 13*i*). Moreover, the tetracerium(III)-bridged $\{W_{44}\}$ unit in the latter is constructed from four $\{CeW_{11}\}$ subunits that are connected through O—Ce—O bonds (Chen, Wang *et al.*, 2014). It is also worth noting that the $\{W_{11}\}$ fragment in $[Ce_4(H_2O)_{12}W_{44}O_{144}(OH)_{12}]^{24-}$ is distinct from the above-mentioned $\{W_{11}\}$ fragment (Fig. 13*j*).

3.4. The progress on IPOMDs

The increasing efforts towards modifying iso-POTs with covalently attached organometallic moieties have led to remarkable progress in IPOMDs and some typical structures of this subset are highlighted here. Among them, iso-POT-based organoruthenium derivatives have been widely studied because of their catalytic applications resulting from the incorporation of highly redox-active ruthenium. In 2001, Proust and co-workers reported a series of IPOTDs, *i.e.* $[\{Ru(\eta^6\text{-}C_6Me_6)\}_4W_4O_{16}]$, $[\{Ru(\eta^6\text{-}C_6Me_6)\}_2W_5O_{18}\{Ru(\eta^6\text{-}$

$C_6Me_6)(H_2O)$}] and [{Ru(η^6-*p*-$MeC_6H_4{}^iPr$)}$_2$(μ-OH)$_3$]$_2$[{Ru(η^6-*p*-$MeC_6H_4{}^iPr$)}$_2W_8O_{28}$(OH)$_2${Ru(η^6-*p*-$MeC_6H_4{}^iPr$)(H_2O)}$_2$] containing [Ru(arene)]$^{2+}$ units (arene = pcymene, C_6Me_6) through the assembly of [{Ru(arene)Cl_2}$_2$] with $WO_4{}^{2-}$ in aqueous or nonaqueous solvents (Artero *et al.*, 2001). Among them, the windmill-like cluster [{Ru(η^6-C_6Me_6)}$_4W_4O_{16}$] (Fig. 14*a*) consists of a $[W_4O_{16}]^{8-}$ anion that supports four [(η^6-C_6Me_6)Ru]$^{2+}$ cations; the structure of the [{Ru(η^6-C_6Me_6)}$_2W_5O_{18}${Ru(η^6-C_6Me_6)(H_2O)}] cluster (Fig. 14*b*) can be described as a central lacunary Lindqvist-type $[W_5O_{18}]^{6-}$ core connecting with three [Ru(arene)]$^{2+}$ moieties; moreover, the centrosymmetric dimeric cluster [{Ru(η^6-*p*-MeC_6H_4-^{i}Pr)}$_2$(μ-OH)$_3$]$_2$[{Ru(η^6-*p*-$MeC_6H_4{}^iPr$)}$_2W_8O_{28}$(OH)$_2${Ru(η^6-*p*-$MeC_6H_4{}^iPr$)(H_2O)}$_2$] (Fig. 14*c*) is made up of two crystallographically equivalent cubane-like [{Ru(arene)}(WO_3)$_3$(μ_3-O)$_3$(μ_3-OH)]$^{5-}$ units linked together by two *cis*-{WO_2}$_2$ groups. In addition, their UV–Vis spectra display two metal-to-ligand charge-transfer transitions between 300 and 450 nm and ligand-to-metal charge-transfer transitions in the higher energy region. In 2013, the diorganoruthenium-supported iso-POT [{Ru(C_6H_6)}$_2W_8O_{28}$(OH)$_2$]$^{6-}$ (Fig. 14*d*) were successfully isolated by Bi *et al.* and consists of two [Ru(C_6H_6)]$^{2+}$ cations linking to a $[W_8O_{28}(OH)_2]^{10-}$ fragment *via* three Ru—O*W* bonds, resulting in an assembly with C_2 symmetry (Meng *et al.*, 2013). Notably, by anchoring on (3-aminopropyl)triethoxysilane (apts) modified SBA-15, this compound exhibits higher catalytic activity in the oxidation of *n*-hexadecane in air without any additives and solvents in comparison with previously reported Ru-containing POTs. In 2004, Kortz's group used the one-pot procedure in the buffer medium and synthesized the Ru-containing iso-POT [$HW_9O_{33}Ru^{II}{}_2$-(dmso)$_6$]$^{7-}$ (dmso is dimethyl sulfoxide; Fig. 14*e*) based on an

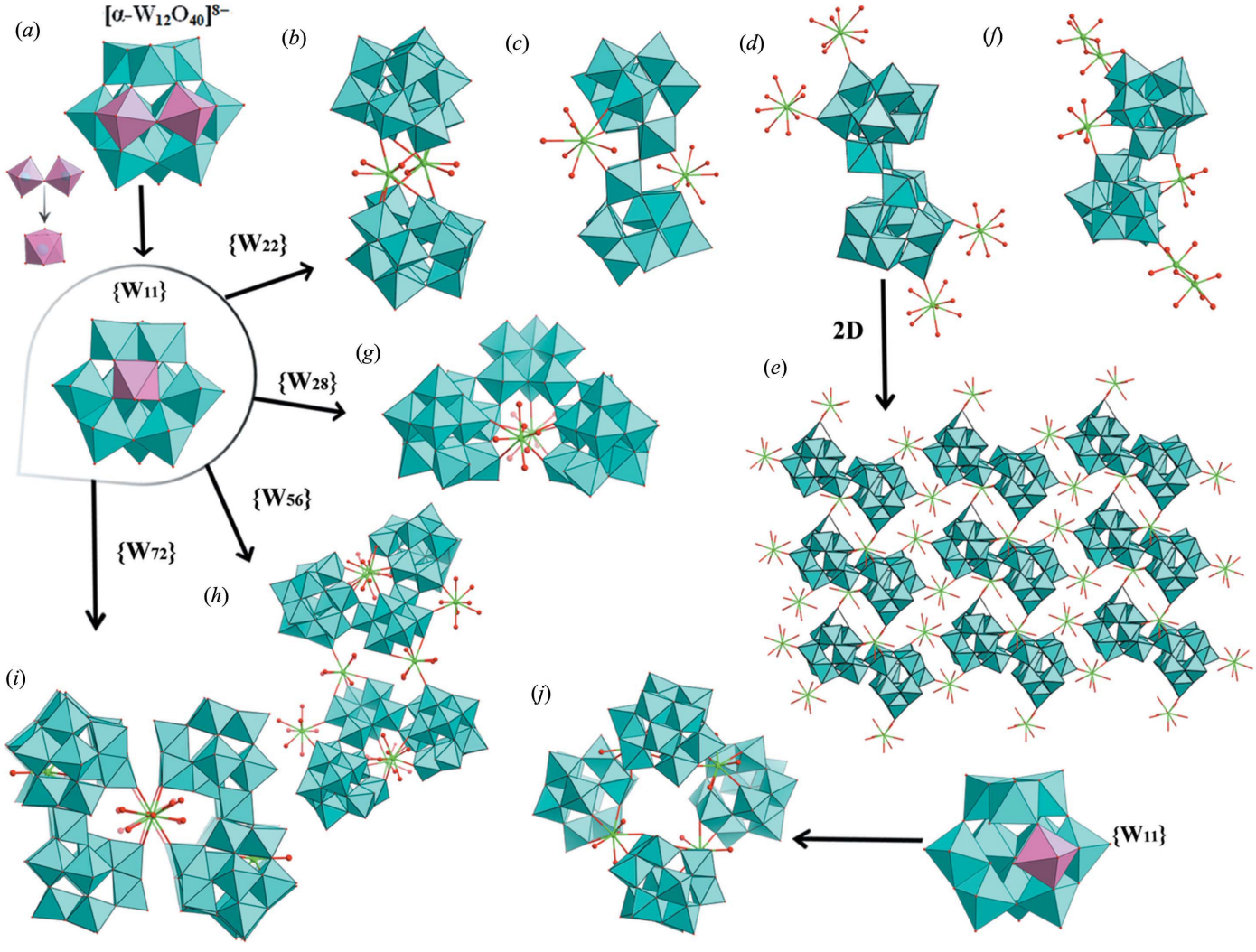

Figure 13
(*a*) The imaginary forming process of the {W_{11}} unit derived from [α-$W_{12}O_{40}$]$^{8-}$. (*b*) The dicerium(III)-bridged {W_{22}} iso-POT [$Ce_2(H_2O)_6W_{22}O_{72}(OH)_4$]$^{10-}$. (*c*) The structure of IPRED [$RE_2(H_2O)_{10}W_{22}O_{71}(OH)_2$]$^{8-}$. (*d*) The structure of IPRED {[$Eu(H_2O)_7$]$_2$[$Eu(H_2O)_5$]$_2$[$W_{22}O_{74}H_2$]}$^{2-}$. (*e*) The 2D sheet structure of {[$Eu(H_2O)_7$]$_2$[$Eu(H_2O)_5$]$_2$[$W_{22}O_{74}H_2$]}$^{2-}$. (*f*) The structure of IPRED {[$RE(H_2O)_4$][$RE(H_2O)_5$]$_2$[$W_{22}O_{74}H_2$]}$^{5-}$. (*g*) The V-shaped {W_{28}} unit [$Ce_2(H_2O)_{10}W_{28}O_{92}(OH)_2$]$^{12-}$. (*h*) The IPRED [$RE_4(H_2O)_{22}W_{28}O_{94}H_2$]$_2^{12-}$. (*i*) The structure of IPRED [$Ce_2(H_2O)_9W_{36}O_{110}$-$(OH)_{12}$]$_2^{20-}$. (*j*) The IPRED [$Ce_4(H_2O)_{12}W_{44}O_{144}(OH)_{12}$]$^{24-}$. Colour key: WO_6 blue, O red and RE green.

$[HW_9O_{33}]^{11-}$ wheel and two $[Ru(dmso)_3]^{2+}$ groups (Bi *et al.*, 2004), which represents the first structurally characterized organoruthenium-coordinated POT in POM chemistry. What is more, Wang and collaborators also reported a tris(2,2′-bpy)ruthenium IPOMD $[Ru(bpy)_3]_2[W_{10}O_{32}]\cdot 3DMSO$ (Fig. 14*f*) by reaction of chiral $[Ru(bpy)_3]^{2+}$ cations and decatungstate $[W_{10}O_{32}]^{4-}$ polyanions in a mixed solvent (Han *et al.*, 2001). Inspired by previous innovative work, Kortz's group also prepared the first dimethyltin-containing IPOMD $[\{(CH_3)_2Sn\}_2(W_6O_{22})]^{4-}$ (Fig. 14*g*), which is composed of a new type of hexatungstate fragment, $[W_6O_{22}]^{8-}$, stabilized by two dimethyltin groups and exhibiting an intriguing 1D arrangement *via* distorted trigonal–bipyramidal *cis*-$(CH_3)_2SnO_3$ moieties (Fig. 14*h*) (Reinoso *et al.*, 2006). By treating WO_4^{2-} with $M(CO)_5Br$ (M = Mn^I and Re^I) in acidic solution in the dark, three novel octatungstate-supported tricarbonyl metal derivatives, *i.e.* $\{[H_2W_8O_{30}][OM(CO)_3]_2\}^{n-}$ (OM^I = Mn^I and n = 8; OM^I = Re^I and n = 4) and $[Mn(H_2O)_2]\{[H_2W_8O_{30}][Mn(CO)_3]_2\}^{6-}$, were synthesized and characterized by Niu *et al.* (2011). It is interesting to note that the $\{[H_2W_8O_{30}][OM(CO)_3]_2\}^{n-}$ unit (Fig. 14*i*) can be considered as an octatungstate $[H_2W_8O_{30}]^{8-}$ polyoxoanion capped by two $[OM(CO)_3]^+$ pendants *via* six μ_2-O atoms and further forms a 1D chain structure with the help of two $[Na_2(H_2O)_8]^{2+}$ clusters (Fig. 14*j*), while, the $[Mn(H_2O)_2]\{[H_2W_8O_{30}][Mn(CO)_3]_2\}^{6-}$ clusters (Fig. 14*k*) are also linked to each other by octahedral $[Mn(H_2O)_2]^{2+}$ cations to generate a 1D chain arrangement (Fig. 14*l*) which further coordinates to $[Na_2(H_2O)_6]^{2+}$ and $[Na_4(H_2O)_{10}]^{4+}$ cations to construct an intriguing 3D structure.

3.5. The progress on IPHMD

To date, only one IPHMD has been reported. In 2008, the novel iso-POT-based 4*d*–4*f* heterometallic compound $[\{Ag_3(H_2O)_2\}\{Ce_2(H_2O)_{12}\}\subset\{H_2W_{11}Ce(H_2O)_4O_{39}\}_2]^{5-}$ was synthesized by Chen's group by reaction of $[H_2W_{12}O_{40}]^{6-}$, Ce^{3+} and Ag^+ in a 1:2:2 ratio in aqueous solution (Fig. 15*a*) (Pang *et al.*, 2008). Intriguingly, adjacent molecular units are linked by Ce^{3+} and Ag^+ cations to form a 2D network (Fig. 15*b*), and such networks are further combined *via* Ag—Ag bonds, generating a purely inorganic 3D framework with two kinds of channels in the [010] and [100] directions (Figs. 15*c* and 15*d*). It is worth mentioning that this compound

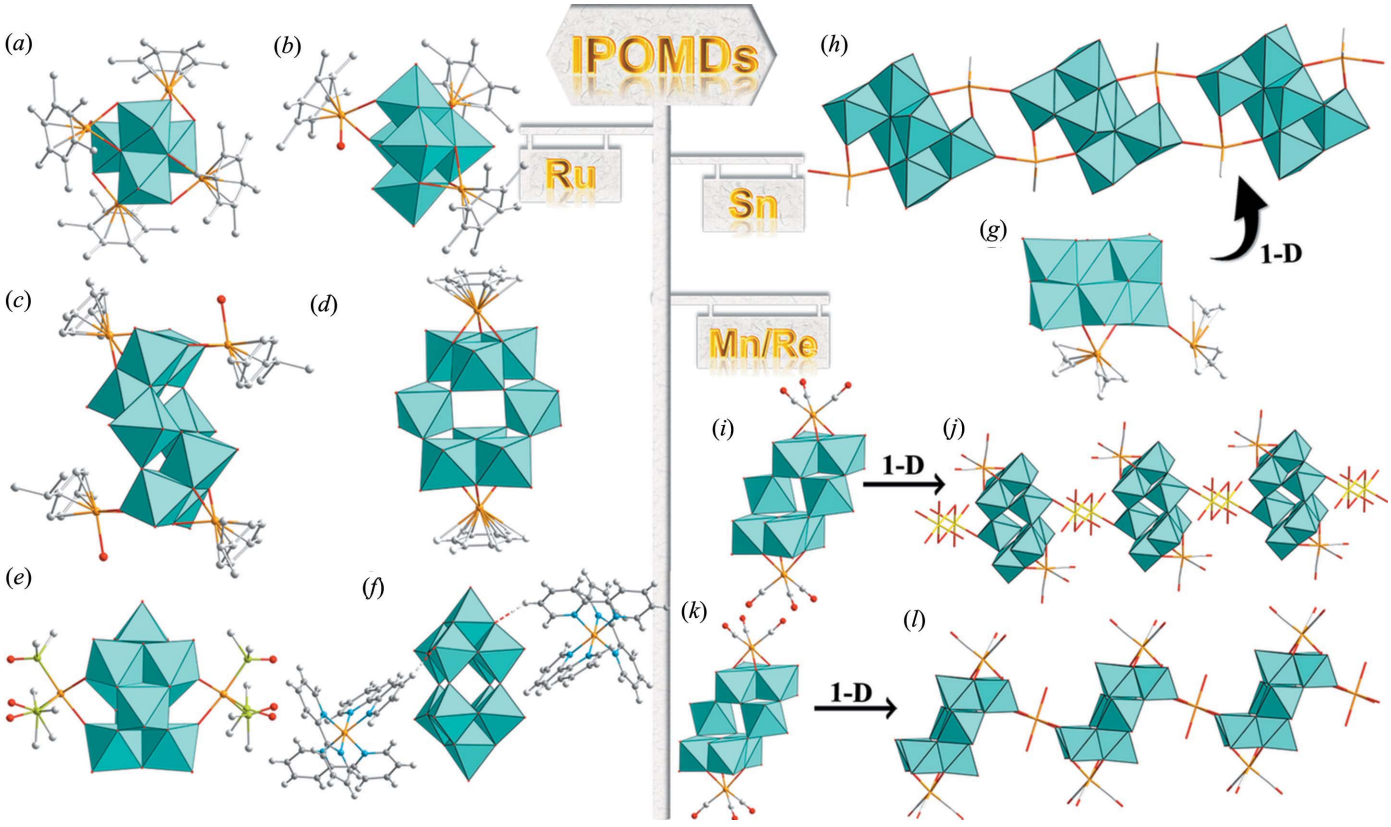

Figure 14
(*a*) The windmill-like cluster $[\{Ru(\eta^6\text{-}C_6Me_6)\}_4W_4O_{16}]$. (*b*) The structure of $[\{Ru(\eta^6\text{-}C_6Me_6)\}_2W_5O_{18}\{Ru(\eta^6\text{-}C_6Me_6)(H_2O)\}]$. (*c*) The centrosymmetric dimeric cluster $[\{Ru(\eta^6\text{-}p\text{-}MeC_6H_4{}^iPr)\}_2(\mu\text{-}OH)_3]_2[\{Ru(\eta^6\text{-}p\text{-}MeC_6H_4{}^iPr)\}_2W_8O_{28}(OH)_2\{Ru(\eta^6\text{-}p\text{-}MeC_6H_4{}^iPr)(H_2O)\}_2]$. (*d*) The diorganoruthenium-supported iso-POT $[\{Ru(C_6H_6)\}_2W_8O_{28}(OH)_2]^{6-}$. (*e*) The nona-isopolytungstate $[HW_9O_{33}Ru^{II}{}_2(dmso)_6]^{7-}$. (*f*) The structure of IPOMD $[Ru(bpy)_3]_2[W_{10}O_{32}]\cdot 3DMSO$. (*g*) The first dimethyltin-containing IPOMD $[\{(CH_3)_2Sn\}_2(W_6O_{22})]^{4-}$. (*h*) The 1D arrangement of $[\{(CH_3)_2Sn\}_2(W_6O_{22})]^{4-}$. (*i*) The tricarbonyl-metal-containing IPOMD $\{[H_2W_8O_{30}][OM(CO)_3]_2\}^{n-}$ (OM^I = Mn^I and n = 8; OM^I = $Re^I$and n = 4). (*j*) The 1D chain-like structure of $\{[H_2W_8O_{30}][OM(CO)_3]_2\}^{n-}$ (OM^I = $Mn^I$and n = 8; OM^I = Re^I and n = 4). (*k*) The tricarbonyl-metal-containing IPOMD $[Mn(H_2O)_2]\{[H_2W_8O_{30}][Mn(CO)_3]_2\}^{6-}$. (*l*) The 1D chain-like structure of $[Mn(H_2O)_2]\{[H_2W_8O_{30}][Mn(CO)_3]_2\}^{6-}$. Colour key: WO_6 blue, O red, OM orange, C grey, S yellow–green and Na yellow.

represents the first inorganic high-dimensional framework based on 4*d*–4*f* heterometals and iso-POTs. Moreover, it also exhibits an excellent reversible water sorption capability, resulting from the loss of coordination water and the probable collapse of the porous frameworks in its structure.

4. Conclusions and future outlook

This review summarizes recent progress in the rapidly developing field of iso-POT-based crystalline materials. On the basis of successful synthetic methods, a large number of iso-POT-based derivatives with diverse structural types and various nuclearities were classified. During the course of the synthesis of these iso-POT-based crystalline materials, the conventional aqueous method was proved to be an effective preparation method, especially for the construction of gigantic iso-POTs, and is still widely utilized to create many other iso-POT-based derivatives. Also, the hydro(solvo)thermal technique has been employed in this field and several unprecedented organic–inorganic hybrid iso-POT-based derivatives with aesthetic topologies have been acquired, proving that it is an effective way to make organic–inorganic hybrid iso-POT-based derivatives. What is more, some effective synthetic strategies, such as the one-pot reaction strategy of simple starting materials, the stepwise synthetic strategy utilizing preformed precursors as building blocks, and alkali-metal-directing self-assembly and pH-controlled self-assembly have been constantly and intensively attempted in the preparation of iso-POT-based derivatives. In this review, we highlight the structural types of iso-POT building blocks, the structural characteristics and the linking modes of different compositions in these compounds. At the same time, some interesting and important properties are also presented.

Although significant progress has been made, there is still a great deal of research potential for the development of iso-POT-based crystalline materials. To date, the nuclearity of the structurally known iso-POTs is still far less known than the hetero-POTs and polymolybdates and the number of iso-POT-based extended materials is limited compared with metal–organic frameworks. Based on the above-mentioned results, several personal viewpoints are presented to help researchers grasp the possibilities for future development of novel iso-POT-based crystalline materials.

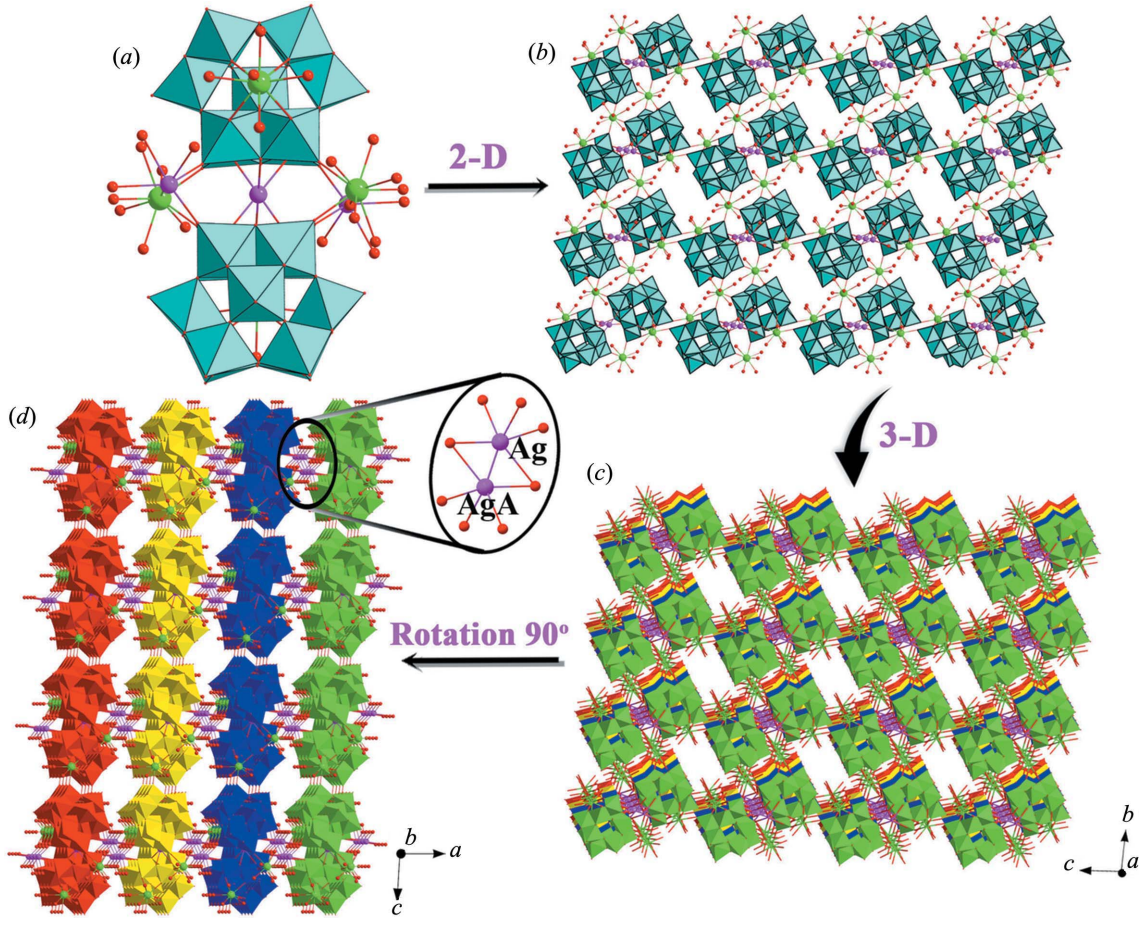

Figure 15
(*a*) The iso-POT-based 4*d*–4*f* heterometallic compound $[\{Ag_3(H_2O)_2\}\{Ce_2(H_2O)_{12}\}\subset\{H_2W_{11}Ce(H_2O)_4O_{39}\}_2]^{5-}$. (*b*) The 2D sheet structure of $[\{Ag_3(H_2O)_2\}\{Ce_2(H_2O)_{12}\}\subset\{H_2W_{11}Ce(H_2O)_4O_{39}\}_2]^{5-}$. (*c*) The inorganic 3D framework of $[\{Ag_3(H_2O)_2\}\{Ce_2(H_2O)_{12}\}\subset\{H_2W_{11}Ce(H_2O)_4O_{39}\}_2]^{5-}$, viewed along the *a* axis. (*d*) The inorganic 3D framework of $[\{Ag_3(H_2O)_2\}\{Ce_2(H_2O)_{12}\}\subset\{H_2W_{11}Ce(H_2O)_4O_{39}\}_2]^{5-}$, viewed along the *b* axis. The atom with the suffix A is generated by the symmetry operation $(-x+1, -y+2, -z)$. Colour key: WO_6 blue, O red, TM pink and RE green.

(i) Other synthetic methods should be introduced and developed in the future. In addition to the conventional aqueous synthetic method and the hydrothermal technology, the mixed-solvent diffusion method, ionothermal synthesis, microwave synthesis and solid-phase synthesis are still in their early stage of application in the field of iso-POT chemistry, which is expected to be exploited in the preparations of iso-POM-based derivatives with fascinating structures and attractive properties.

(ii) Introduction of various precursors should be attempted. As can be seen from the aforementioned examples, the precursors which are mainly used in the synthesis of iso-POT-based derivatives are limited, such as $[W_6O_{19}]^{2-}$, $[W_{10}O_{32}]^{4-}$ and $[H_2W_{12}O_{40}]^{6-}$. Thus, there is indeed further potential to explore and prepare more iso-POT precursors utilized for the preparation of iso-POM-based derivatives. What is more, the combination of iso-POT building blocks with as-synthesized TM/RE clusters (for instance, $\{Fe_{10}\}$, $\{Fe_{12}\}$, $\{Ag_{20}\}$ and $\{Dy_{10}\}$) may also be an efficient way to obtain high-nuclear nanosized iso-POT-based derivatives (Koumousi *et al.*, 2013; Li *et al.*, 2018; Westin *et al.*, 2003), which has already been confirmed by Fang's illuminating work on the assembly of the magnetic cluster $\{Mn_{14}W_{48}\}$ (Fang & Luban, 2011).

(iii) Multifunctional organic components in the construction of iso-POT-based crystalline materials are also introduced, albeit their poor solubility makes the preparation of organic–inorganic hybrid iso-POT-based derivatives a challenging task. On one hand, the introduction of organic ligands into iso-POT clusters will improve their biological activity and reduce their toxicity, as POMs usually exhibit promising applications in medicine and biology. On the other hand, the organic ligands can participate in coordination with iso-POT clusters, giving access to organic-ligand-decorated iso-POT materials, which will greatly expand their applications, especially in molecular recognition, catalysis and gas adsorption.

We believe that further in-depth research on iso-POT-based derivatives can not only provide valuable guidance to ongoing developments in exploring and discovering novel functional iso-POTs, but also gradually highlight the importance of the iso-POT branch in the frontier area of POM chemistry.

Funding information

Funding for this research was provided by: Natural Science Foundation of China (grant Nos. 21571048, 21671054 and 21771052), the Program for Science & Technology Innovation Talents in Universities of Henan Province (grant No. 16HASTIT001), the Innovation Scientists and Technicians Troop Construction Projects of Henan Province (grant No. 174100510016) and the Students Innovative Pilot Plan of Henan University (grant No. 16NA005).

References

Allmann, R. (1971). *Acta Cryst.* B**27**, 1393–1404.
Almeida Paz, F. A., Balula, M. S. S., Cavaleiro, A. M. V., Klinowski, J. & Nogueira, H. I. S. (2005). *Acta Cryst.* E**61**, i28–i31.
Artero, V., Proust, A., Herson, P. & Gouzerh, P. (2001). *Chem. Eur. J.* **7**, 3901–3910.
Bhattacharyya, R., Biswas, S., Armstrong, J. & Holt, E. M. (1989). *Inorg. Chem.* **28**, 4297–4300.
Bi, L., Hussain, F., Kortz, U., Sadakane, M. & Dickman, M. H. (2004). *Chem. Commun.* **12**, 1420–1421.
Brüdgam, I., Fuchs, J., Hartl, H. & Palm, R. (1998). *Angew. Chem. Int. Ed.* **37**, 2668–2671.
Cameron, J. M., Gao, J., Long, D.-L. & Cronin, L. (2014). *Inorg. Chem. Front.* **1**, 178–185.
Chen, W.-C., Li, H.-L., Wang, X.-L., Shao, K.-Z., Su, Z.-M. & Wang, E.-B. (2013). *Chem. Eur. J.* **19**, 11007–11015.
Chen, W.-C., Wang, X.-L., Jiao, Y.-Q., Huang, P., Zhou, E.-L., Su, Z.-M. & Shao, K.-Z. (2014). *Inorg. Chem.* **53**, 9486–9497.
Chen, W.-C., Yan, L.-K., Wu, C.-X., Wang, X.-L., Shao, K.-Z., Su, Z.-M. & Wang, E.-B. (2014). *Cryst. Growth Des.* **14**, 5099–5110.
Chi, Y.-N., Shen, P.-P., Cui, F.-Y., Lin, Z.-G., Chen, S.-L. & Hu, C.-W. (2014). *Inorg. Chem.* **53**, 5029–5036.
Coppens, P., Chen, Y. & Trzop, E. (2014). *Chem. Rev.* **114**, 9645–9661.
Devi, R. N., Burkholder, E. & Zubieta, J. (2003). *Inorg. Chim. Acta*, **348**, 150–156.
Du, D.-Y., Yan, L.-K., Su, Z.-M., Li, S.-L., Lan, Y.-Q. & Wang, E.-B. (2013). *Coord. Chem. Rev.* **257**, 702–717.
Fang, X. & Luban, M. (2011). *Chem. Commun.* **47**, 3066–3068.
Fang, W.-H., Zhang, L. & Zhang, J. (2017). *Chem. Soc. Rev.* **47**, 404–421.
Fuchs, J. & Flindt, E.-P. (1979). *Z. Naturforsch. Teil B*, **34**, 412–422.
Fuchs, J., Freiwald, W. & Hartl, H. (1978). *Acta Cryst.* B**34**, 1764–1770.
Fuchs, J., Palm, R. & Hartl, H. (1996). *Angew. Chem. Int. Ed. Engl.* **35**, 2651–2653.
Gao, J., Yan, J., Beeg, S., Long, D.-L. & Cronin, L. (2012). *Angew. Chem. Int. Ed.* **51**, 3373–3376.
Han, Q., Sun, X., Li, J., Ma, P. & Niu, J. (2014). *Inorg. Chem.* **53**, 6107–6112.
Han, Z., Wang, E., Luan, G., Li, Y., Hu, C., Wang, P., Hu, N. & Jia, H. (2001). *Inorg. Chem. Commun.* **4**, 427–429.
Hartl, H., Palm, R. & Fuchs, J. (1993). *Angew. Chem. Int. Ed. Engl.* **10**, 1492–1494.
Hashimoto, M., Iwamoto, T., Ichida, H. & Sasaki, Y. (1991). *Polyhedron*, **10**, 649–651.
Hill, C. L. (1998). *Chem. Rev.* **98**, 1–2.
Ismail, A. H., Bassil, B. S., Suchopar, A. & Kortz, U. (2009). *Eur. J. Inorg. Chem.* pp. 5247–5252.
Ismail, A. H., Dickman, M. H. & Kortz, U. (2009). *Inorg. Chem.* **48**, 1559–1565.
Kortz, U., Müller, A., Slageren, J. v., Schnack, J., Dalal, N. S. & Dressel, M. (2009). *Coord. Chem. Rev.* **253**, 2315–2327.
Koumousi, E. S., Routzomani, A., Nguyen, T. N., Giannopoulos, D. P., Raptopoulou, C. P., Psycharis, V., Christou, G. & Stamatatos, T. C. (2013). *Inorg. Chem.* **52**, 1176–1178.
Lehmann, T. & Fuchs, J. Z. (1988). *Z. Naturforsch. Teil B*, **43**, 89–93.
Li, B., Bi, L., Li, W. & Wu, L. (2008). *J. Solid State Chem.* **181**, 3337–3343.
Li, S., Du, X.-S., Li, B., Wang, J.-Y., Li, G.-P., Gao, G.-G. & Zang, S.-Q. (2018). *J. Am. Chem. Soc.* **140**, 594–597.
Li, Y., Leng, C., Zhao, J., Chen, S., Ma, P. & Chen, L. (2012). *Inorg. Chem. Commun.* **25**, 35–38.
Li, T.-H., Li, F., Lu, J., Guo, Z.-G., Gao, S.-Y. & Cao, R. (2008). *Inorg. Chem.* **47**, 5612–5615.
Li, H.-L., Liu, Y.-J., Zheng, R., Ma, X., Chen, L.-J. & Zhao, J.-W. (2017). *Spectrochim. Acta Part A*, **176**, 114–122.
Li, Y., Wang, E., Wang, S., Lu, Y., Hu, C., Hu, N. & Jia, H. (2002). *J. Mol. Struct.* **607**, 133–141.
Li, H., Yang, W., Wang, X., Chen, L., Ma, J., Zheng, L. & Zhao, J. (2016). *Cryst. Growth Des.* **16**, 108–120.
Lin, B.-Z., Chen, Y.-M. & Liu, P.-D. (2003). *Dalton Trans.* pp. 2474–2477.

Lis, T. (1980). *Acta Cryst.* B**36**, 2042–2046.
Liu, J., Han, Q., Chen, L. & Zhao, J. (2016). *CrystEngComm*, **47**, 842–862.
Liu, C., Luo, F., Liu, N., Cui, Y., Wang, X., Wang, E. & Chen, J. (2006). *Cryst. Growth Des.* **6**, 2658–2660.
Long, D.-L., Abbas, H., Kögerler, P. & Cronin, L. (2004). *J. Am. Chem. Soc.* **126**, 13880–13881.
Long, D.-L., Brücher, O., Streb, C. & Cronin, L. (2006). *Dalton Trans.* pp. 2852–2860.
Long, D.-L., Burkholder, E. & Cronin, L. (2007). *Chem. Soc. Rev.* **36**, 105–121.
Long, D.-L., Kögerler, P., Parenty, A. D. C., Fielden, J. & Cronin, L. (2006). *Angew. Chem. Int. Ed.* **45**, 4798–4803.
Long, D.-L., Tsunashima, R. & Cronin, L. (2010). *Angew. Chem. Int. Ed.* **49**, 1736–1758.
Ma, P., Hu, F., Wang, J. & Niu, J. (2018). *Coord. Chem. Rev.* doi: 10.1016/j.ccr.2018.02.010.
Ma, X., Li, H., Chen, L. & Zhao, J. (2016). *Dalton Trans.* **45**, 4935–4960.
Ma, X., Yang, W., Chen, L. & Zhao, J. (2015). *CrystEngComm*, **17**, 8175–8197.
Meng, R.-Q., Wang, B., Sui, H.-M., Li, B., Song, W., Wu, L.-X., Zhao, B. & Bi, L.-H. (2013). *Eur. J. Inorg. Chem.* pp. 1935–1942.
Miras, H. N., Yan, J., Long, D.-L. & Cronin, L. (2008). *Angew. Chem. Int. Ed.* **47**, 8420–8423.
Mitchell, S. G., Boyd, T., Miras, H. N., Long, D.-L. & Cronin, L. (2011). *Inorg. Chem.* **50**, 136–143.
Niu, J.-Y., Yang, L.-P., Zhao, J.-W., Ma, P.-T. & Wang, J.-P. (2011). *Dalton Trans.* **40**, 8298–8300.
Oliva, A. R. d. l., Sans, V., Miras, H. N., Yan, J., Zang, H., Richmond, C. J., Long, D.-L. & Cronin, L. (2012). *Angew. Chem. Int. Ed.* **51**, 12759–12762.
Oms, O., Dolbecq, A. & Mialane, P. (2012). *Chem. Soc. Rev.* **41**, 7497–7536.
Pang, H., Zhang, C., Shi, D. & Chen, Y. (2008). *Cryst. Growth Des.* **8**, 4476–4480.
Peacock, R. D. & Weakley, T. J. R. (1971). *J. Chem. Soc. A*, pp. 1836–1839.
Reinoso, S., Bassil, B. S., Barsukova, M. & Kortz, U. (2010). *Eur. J. Inorg. Chem.* pp. 2537–2542.
Reinoso, S., Dickman, M. H. & Kortz, U. (2006). *Inorg. Chem.* **45**, 10422–10424.
Rodriguez-Albelo, L. M., Ruiz-Salvador, A. R., Sampieri, A., Lewis, D. W., Gómez, A., Nohra, B., Mialane, P., Marrot, J., Sécheresse, F., Mellot-Draznieks, C., Biboum, R. N., Keita, B., Nadjo, L. & Dolbecq, A. (2009). *J. Am. Chem. Soc.* **131**, 16078–16087.
Rozes, L. & Sanchez, C. (2011). *Chem. Soc. Rev.* **40**, 1006–1030.
Song, L.-Y., Zhang, D.-D., Ma, P.-T., Liang, Z.-J., Wang, J.-P. & Niu, J.-Y. (2013). *CrystEngComm*, **15**, 4597–4600.
Sprangers, C. R., Marmon, J. K. & Duncan, D. C. (2006). *Inorg. Chem.* **45**, 9628–9630.
Stomberg, R. (1985). *Acta Chem. Scand. Ser. A*, **39**, 507–514.
Streb, C., McGlone, T., Brücher, O., Long, D.-L. & Cronin, L. (2008). *Chem. Eur. J.* **14**, 8861–8868.
Suzuki, H., Hashimoto, M. & Okeya, S. (2004). *Eur. J. Inorg. Chem.* pp. 2632–2634.
Westin, L. G., Kritikos, M. & Caneschi, A. (2003). *Chem. Commun.* pp. 1012–1013.
Wu, H.-L., Zhang, Z.-M., Li, Y.-G., Wang, X.-L. & Wang, E.-B. (2015). *CrystEngComm*, **17**, 6261–6268.
Xin, F. & Pope, M. T. (1996). *J. Am. Chem. Soc.* **118**, 7731–7736.
Zhan, C.-H., Winter, R. S., Zheng, Q., Yan, J., Cameron, J. M., Long, D.-L. & Cronin, L. (2015). *Angew. Chem. Int. Ed.* **54**, 1–6.
Zhang, Z.-M., Duan, X., Yao, S., Wang, Z., Lin, Z., Li, Y.-G., Long, L.-S., Wang, E.-B. & Lin, W. (2016). *Chem. Sci.* **7**, 4220–4229.
Zhao, J.-W., Li, Y.-Z., Chen, L.-J. & Yang, G.-Y. (2016). *Chem. Commun.* **52**, 4418–4445.
Zhao, J., Li, H., Li, Y., Li, C., Wang, Z. & Chen, L. (2014). *Cryst. Crowth Des.* **14**, 5495–5505.
Zhao, J.-W., Li, H.-L., Ma, X., Xie, Z., Chen, L.-J. & Zhu, Y. (2016). *Sci. Rep.* **6**, 26406.
Zheng, S.-T. & Yang, G.-Y. (2012). *Chem. Soc. Rev.* **41**, 7623–7646.